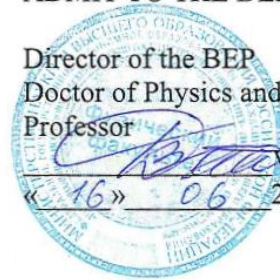


Ministry of Science and Higher Education of the Russian Federation
NATIONAL RESEARCH
TOMSK STATE UNIVERSITY (NR TSU)
Faculty of Physics

ADMIT TO THE DEFENCE AT THE SEB

Director of the BEP
Doctor of Physics and Mathematics,
Professor



[Signature] P. Demkin
« 16 » 06 20 22

MASTER'S THESIS

DEVELOPMENT OF THE MRI-IMAGES ANALYSIS ALGORITHMS BASED ON
GRADIENT METHODS

within the Basic Educational Programme of Master's Degree «Physics Methods and Information
Technologies in Biomedicine»
subject area 03.04.02 – Physics

Altynbekov Almat Altynbekovich

Research supervisor
Cand. Sc. of Physics and
Mathematics, Associate Professor

[Signature] A.V. Borisov

signature
« 15 » 06 20 22

Author

student of group No 052063

[Signature] A.A. Altynbekov
signature

Tomsk–2022

ABSTRACT

The topic of the master's thesis is «Development of the MRI-images analysis algorithms based on gradient methods». The object of the study is an MRI-image of the human brain. Subject of research: the use of gradient methods to improve the quality of classification of MRI-images of the brain. The aim of the master's thesis is to analyze the possibilities of gradient methods used in the processing of magnetic resonance imaging data of the brain.

Tasks of the master's thesis:

- 1) study of the principle of operation of MRI and other methods of medical imaging;
- 2) creation of an algorithm that allows classifying MRI data of patients with various pathologies;
- 3) creation of an approach to improve the classification of MRI data and search for the most optimal parameters for gradient methods used in this approach.

In the master's work, the methods of obtaining brain images and their advantages, segmentation methods, methods for selecting object boundaries and recognition methods are considered. A program for image conversion, image dimensionalization, image analysis and classification has been implemented. The results are shown in illustrations and summarized in a table. The result of the master's work is a program on the analysis and classification of MRI-images.

The work consists of an introduction, three chapters and a conclusion. The total volume of the explanatory note is 51 sheets. The explanatory note contains 22 illustrations, 2 tables and 78 sources and literature used.

CONTENTS

INTRODUCTION.....	5
1 Methods of obtaining brain images.....	7
1.1 Overview of the most common methods of obtaining medical images of the brain	7
1.2 Magnetic resonance imaging.....	12
1.3 Presentation of medical data.....	14
1.4 Methods of image analysis	16
1.4.1 Segmentation methods.....	16
1.4.1.2 Region growing method.....	22
1.4.1.3 Watershed method.....	24
1.4.2 Methods for selecting the boundaries of object.....	26
1.4.3 Multispectral methods.....	30
1.4.4 Clustering.....	33
2 Material and methods.....	34
2.1 Principal component analysis.....	34
2.2 Classification of MRI data for two pathologies	35
3 Development of approaches for the analysis of MRI data and their classifications	37
CONCLUSION	48
REFERENCES	49

LIST OF ABBREVIATIONS

- MRI – Magnetic resonance imaging
- CT – Computer tomography
- PET – Positron emission tomography
- kHz – kiloHertz
- EM – ElectroMagnetic
- kg – kilogram
- NMR – Nuclear magnetic resonance
- mm – millimeter
- DICOM – Digital Imaging and Communications in Medicine
- PACS – Picture Archiving and Communication System
- SPET – Single-photon positron emission tomography
- MRA – Magnetic resonance angiography
- ROI – Reference area of interest
- PCA – Principal component analysis
- FLAIR – Fluid attenuation inversion recovery
- CSF – Cerebrospinal fluid
- SVM – Support vector machine

INTRODUCTION

Currently, there are many methods for obtaining medical images. These methods include MRI, CT, PET and ultrasonography. They are the most used for the diagnosis of the brain, lungs, abdominal cavity, etc.

The use of magnetic resonance imaging (MRI) in the field of medicine and the emergence of radiology are relatively new compared to classical specialties in medicine.

Since its inception, MRI has grown exponentially, leading to the emergence of exciting new areas of research. One of these areas is the use of computational methods for analyzing MRI-images.

In the areas of modern medicine, the field of processing and analysis of visual data is actively developing. Computer technology allows more in-depth analysis of medical images such as computed tomography and magnetic resonance imaging.

Despite the development of modern medical diagnostic equipment, the image that is obtained as a result of diagnostics may not always be clear and with high resolution. Because of this, the field of processing and analysis of visual medical data is actively developing - computer technology that allows you to analyze medical images such as CT, MRI, PET, etc.

Due to the huge amount of visualization data obtained during clinical practice, there are few specialists engaged in uncontrolled (without a teacher) analysis and classification of medical images.

To date, there are many methods for analyzing medical images, which facilitate the study of the physiology of internal organs and the detection of pathologies.

Object of study: MRI-image of the human brain.

Subject of study: gradient methods used to improve the quality of classification of MRI-images of the brain.

The purpose of the master's thesis is to analyze the possibilities of gradient methods used in the processing of data from magnetic resonance imaging of the brain.

Tasks of the master's thesis:

- 1) study of the principle of operation of MRI and other methods of medical imaging;
- 2) creation of an algorithm that allows classifying MRI data of patients with various pathologies;
- 3) creation of an approach to improve the classification of MRI data and search for the most optimal parameters for gradient methods used in this approach.

1 Methods of obtaining brain images

1.1 Overview of the most common methods of obtaining medical images of the brain

This chapter is devoted to an overview of physical methods to obtain a medical image. The most common methods and well-proven are: MRI, CT, ultrasonography, PET.

PET is a radionuclide tomographic method based on the registration of a pair of gamma quanta arising from the annihilation of positrons with electrons [1].

Before the study, a radiopharmaceutical is injected into the patient's body, which further beta decay of the radionuclide occurs and thereby a positron arises. The positron travels a distance before colliding with the electrons of the study environment, then the positron combines with the electron. During the unification, the particles destroy each other, i.e., the process of annihilation occurs and their mass is transformed into energy, leading to the emission of two oppositely directed rays (high-energy photons). The image is formed by moving two detectors and registering two gamma quanta by these detectors as a result of positron annihilation.

The most commonly used isotope is 2-deoxy-2-[fluoro-18]-fluoro-D-glucose (18-FDG), which is a glucose analog in which the hydroxyl group is replaced by fluoro-18. After the injected of the radiopharmaceutical, the isotope is captured by the same mechanism as the capture of ordinary glucose. However, the capture of the isotope stops at the stage of phosphorylation of aerobic glycolysis, the isotope combines with the phosphoric acid residue and remains in the cell.

The physical limitations imposed on the resolution of PET systems are determined by the finiteness of the free path of the positron in the biological tissue, as well as a small deviation of the gamma-ray scattering angle from 180° . It is also possible to combine with CT and MRI.

Contraindications to PET:

- 1) diabetes mellitus;
- 2) severe renal failure;
- 3) pregnancy.

Figure 1 shows an image of the brain obtained by PET.

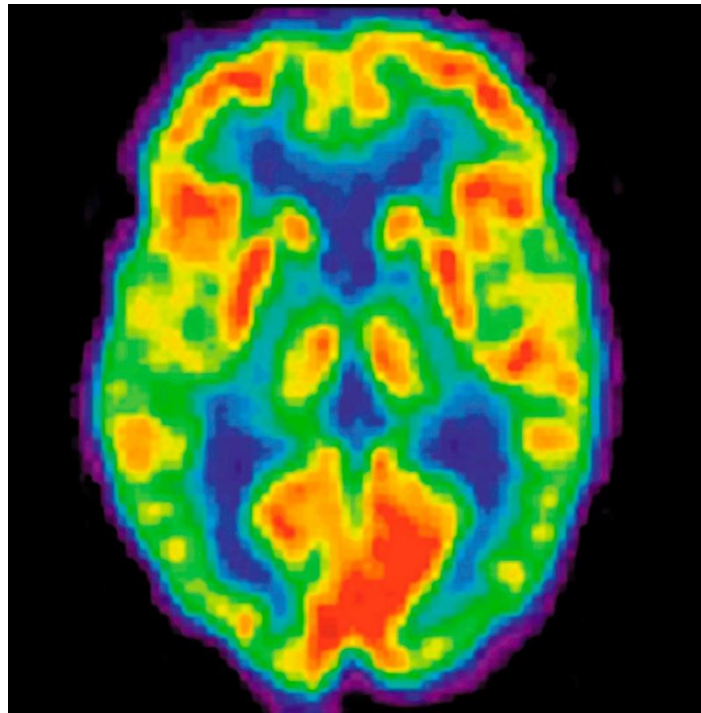


Figure 1– PET image of the human brain

The next method based on the interaction of ultrasound with human tissues is ultrasonography. Ultrasound is a mechanical vibration and waves, the frequency of which is more than 20 kHz. Ultrasound in gases and air, in comparison with liquids and solids, distributed with a large attenuation [2].

The basis of the method is the piezoelectric effect. When the single crystals of some chemical compounds are deformed under the action of ultrasound waves, electric charges opposite in sign appear on the surface of the crystals. When an alternating electric charge is applied to them, mechanical vibrations arise in the crystals with the emission of ultrasonic waves. Thus, the same piezoelectric element can alternately be a receiver or a source of ultrasonic waves.

Imaging obtaining divided into two parts: the first is the emission of short ultrasound pulses directed into the studied tissues; the second is the registration of reflected signals from tissues and organs.

Any environment, including body tissues, prevents the spread of ultrasound, i.e. it has different acoustic resistance, the value of which depends on their density and the speed of distribution of sound waves.

Having reached the boundary of two environment with different acoustic resistance, the beam of ultrasound waves undergoes significant changes: one part of it continues to propagate in a new environment, being absorbed by it to one degree or another, the other is reflected. The

reflection coefficient depends on the difference in the values of the sound resistance of the tissues bordering each other.

Ultrasonography plays an important role in the examination of internal organs, such as: the abdominal cavity and pelvis.

Conducting brain diagnostics by ultrasonography includes the following limitations: low resolution, because the bone structure create interferes or completely excludes conducting ultrasound examination and increasing frequency, the penetrating ability or depth of scanning turns out to be less. This suggests that ultrasonography is not capable of examining an object at a depth of more than 5 cm.

Figure 2 shows the result of scanning the brain with an ultrasonography device (an ultrasonography diagnostic device).

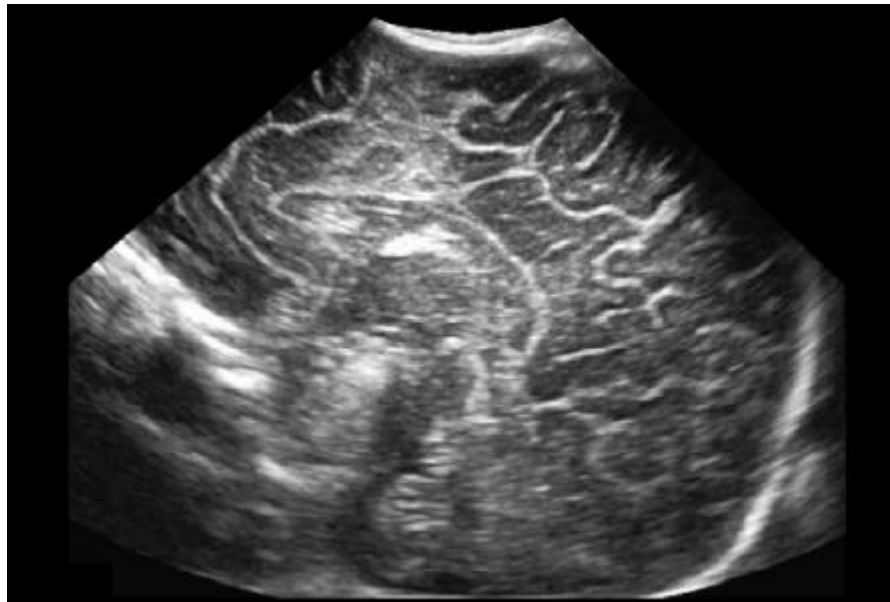


Figure 2 – Ultrasonography image of the human brain

One of the methods based on X-ray irradiation is a computed tomograph. X-rays are EM radiation occupying the spectral region between UV and gamma radiation [3].

The source of X-rays is an X-ray tube, in which there are two electrodes - a cathode and an anode. When the cathode is heated, electron emission occurs. Electrons flying out of the cathode are accelerated by an electric field and hit the surface of the anode. When an electron flies out of the cathode, the electric field causes it to fly towards the anode, while its velocity continuously increases, the electron carries a magnetic field, the intensity of which increases with the electron velocity. Reaching the surface of the anode, the electrons are sharply inhibited, and an electromagnetic pulse with wavelengths in a certain interval (braking radiation) occurs.

The distribution of the radiation intensity over the wavelengths depends on the anode

material and the applied voltage, while on the side of 2 short waves, this curve begins with a certain threshold minimum wavelength, depending on the applied voltage.

The total power of X-ray radiation is 0.1% of the power consumed, since the rest is spent on heat.

During X-ray irradiation of the patient, the absorption and scattering of quanta occurs, thereby weakening occurs. The degree of weakening varies, because organs and tissues have different densities. The X-ray image is based on the uneven absorption of X-ray radiation by various anatomical structures, organs and tissues. Absorption depends on the atomic composition, density and thickness of the object under study, as well as the radiation energy. To the greatest extent, X-ray radiation is absorbed by bones, to a much lesser extent by soft tissues.

Conducting diagnostics by computed tomography includes a number of advantages and disadvantages:

1) exposure to ionizing radiation. Currently, a dose of radiation is used that does not endanger human life. After the first procedure, a period of time should pass for repeated diagnosis. Otherwise, the implementation of repeated diagnostics without a proper break, threatens with bad consequences;

2) absorption of X-rays by solid tissue. These are mainly tissues of considerable density, for example: rays are absorbed to a greater extent in bones, to a lesser extent in soft tissues and body fluids, to an even lesser extent in fatty tissues and gases. This suggests that during the diagnosis of the brain, brain tissue will not be so clearly visible in the image, which in turn makes it difficult to recognize the pathology;

3) the possibility of conducting diagnostics using a contrast agent. A contrast agent is used that absorbs radiation more strongly than the organ under study. Examples of such substances are barium sulfate, organic iodine compounds and gases.

Figure 3 shows an image of a slice of the human brain obtained by computed tomography.

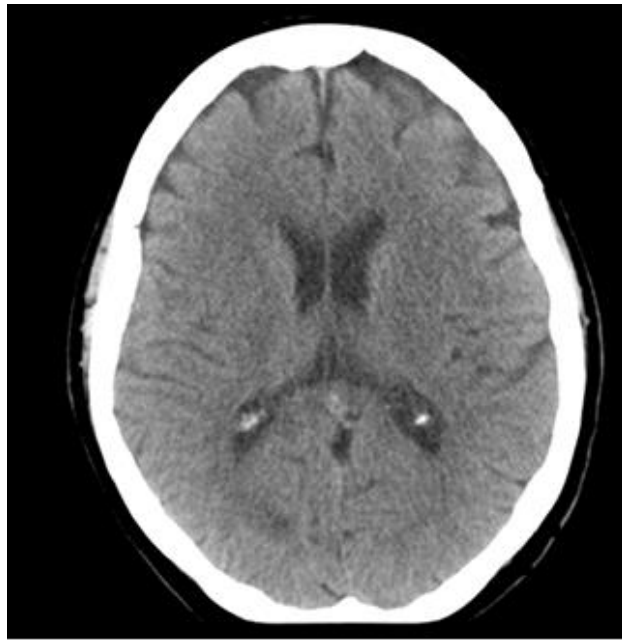


Figure 3– CT image of the human brain

MRI is a method based on the phenomenon of nuclear magnetic resonance, which allows to obtain a high-quality image of the soft tissues of the human body [4].

The phenomenon of nuclear magnetic resonance consists in the resonant absorption or emission of EM energy by a substance whose nuclei have a non-zero magnetic moment. These are the nuclei H^1 , H^2 , C^{13} , N^{14} , F^{19} , Na^{23} , P^{31} .

Under the influence of the magnetic field B_0 , the proton spins of hydrogen nuclei change their position and are located along the axis of the magnetic field B_0 . By the action of the magnetic field B_1 and the radio frequency pulse on the protons of hydrogen nuclei, the proton spins are rearranged relative to new axes for a very short period of time, which is accompanied by the release of energy. Recording this energy is the basis of an MRI-image. Based on the basics of MRI, it can be assumed that it is more informative, especially to soft tissues and does not emit ionizing radiation. It is also possible to combine with a gadolinium-based contrast agent.

The following disadvantages are additionally attributed to MRI:

1) contraindication of the diagnosis of patients with extraneous and implanted metal products or electronic device and the presence of tattoos made with dyes containing a metal compound. For example: pacemaker, hemostatic clips, etc;

2) contraindication of the diagnosis to persons with fever, psychopathological symptom - claustrophobia, with a large excess of scales, about 150 kg.

Figure 4 shows an image of a slice of the human brain obtained by magnetic resonance imaging.

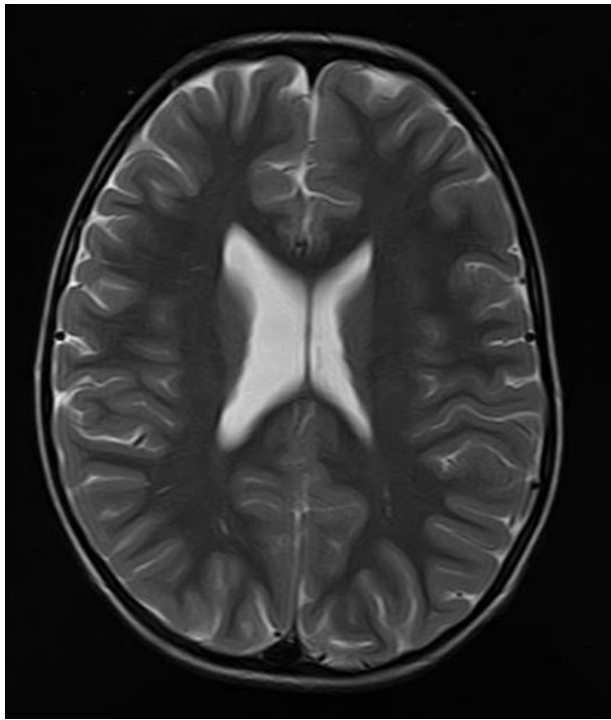


Figure 4 – MRI image of the human brain

1.2 Magnetic resonance imaging

A magnetic resonance image (MRI) is a slice of the object under study and consists of individual plane elements called pixels. A slice consists of individual volume elements or so-called voxels. The volume of each voxel is approximately 3 mm^3 . The pixel intensity is proportional to the intensity of the NMR signal consisting of the voxels of the displayed object.

In NMR tomography, the signal is recorded from resonating nuclei having both spin and magnetic moment. Hydrogen protons H^1 are most often used.

When a proton is placed in an external magnetic field, the spin vector is positioned relative to the external field. Spin also has a low-energy N-S-N-S and a high-energy N-N-S-S state. But in order to cause a transition between two spin states, a photon must have energy

$$E = h\gamma B \quad (1)$$

where h – Planck 's constant, J s;

γ – gyromagnetic ratio, MHz/T;

B – magnetic field voltage, T.

The signal that is recorded during the examination it is obtained from the difference between the absorbed energy of the spins in which there was a transition from a lower energy level to a higher one and the energy emitted by the spins in which there was a transition from a higher level to a lower one.

At any time, the magnetic field corresponding to the spins in each group of spins experiencing the same magnetic field force can be represented by the magnetization vector. The sum of all the magnetization vectors of all spin groups is the total magnetization. To convert to a generally accepted NMR coordinate system, the external magnetic field and the magnetization vector are directed along the z axis.

A change in the total magnetization is possible by exposing the nuclear spin to a frequency energy equal to the energy difference between the spin states. If enough energy has entered the system, it is possible to saturate the spin system and make $M_z=0$ [19].

T_1 time spin-lattice relaxation is a time constant describing how M_z returns to the equilibrium value. This phenomenon is described by an equation that is a function of time t, which after the transformation has the form:

$$M_z = M_0(1 - 2e^{-t/T_1}) \quad (2)$$

where M_0 —equilibrium magnetization;

t —time;

T_1 —spin-lattice relaxation;

M_z —longitudinal magnetization.

T_1 is the time required to reduce the difference between the longitudinal magnetization (M_z) and its equilibrium value with a coefficient e.

If the total magnetization is located in the XY plane, then it will rotate around the Z axis with a frequency that will be equal to the frequency of the photon that causes the transition between the two spin energy states. This frequency is called the Larmor frequency [19].

In addition to rotation, there is a phase shift due to the fact that each spin group experiences a magnetic field different from the magnetic field experienced by other spin groups. The more time passes, the greater the phase difference.

The time constant describing the behavior of transverse magnetization M_{xy} is called the spin-spin relaxation time T_2

$$M_{XY} = M_{XY_0} e^{-t/T_2} \quad (3)$$

where M_{xy} —transverse magnetization;

t —time;

T_2 —spin-spin relaxation;

M_{XY_0} —equilibrium magnetization.

T_2 is always less than T_1 . The total magnetization of the XY axes tends to zero, then the longitudinal magnetization increases until M_0 is along the Z axis.

The contrast of the received images is affected by the time TR (determines the level of tissue saturation or the effect of the T_1 relaxation process) and the time TE (determines the level of dephasing until the echo signal is read or the effect of the T_2 relaxation process).

1.3 Presentation of medical data

With the development of computer technologies in medicine, it became necessary to create unified international standards for the exchange of medical data. There are many different medical standards: ASTM, ASC X12, IEEE/MEDIX, NCPDP, HL7, DICOM, etc. Currently, the main medical communication standard for image transmission is DICOM [5].

DICOM (Digital Imaging and Communications in Medicine, Digital Images and their Exchange in Medicine) is a standard for transferring images and other medical information between computers, based on the Open System Interconnection (OSI) standard developed by the International Standards Organization. DICOM can be used in network environments using standard protocols, for example TCP/IP [6].

The standard has a technology for the unique identification of any information object during network interaction, applies image compression according to the JPEG standard. Having appeared as a corporate, DICOM has become a de facto standard and is integrated into the equipment of the largest manufacturers of radiological equipment and most PACS systems [5].

The file storing one image in the DICOM standard includes not only the image but also some information: data about the equipment on which the study was conducted; a description of the study; parameters and description of the series; coordinate systems associated with the image; attributes defining the image itself; text and graphic elements, graphs and comments performed by medical personnel and attributes describing the transformation over the received

data, etc. A separate DICOM file contains both the header (which stores information about the patient's name, type of study, image size, etc.) and all image data (which can contain information in three dimensions). Another difference of DICOM is that DICOM image data can be compressed to reduce the image size, resulting in data loss.

The element defining the transfer syntax is important. It talks about the data structure of the image, showing whether the data has been compressed. DICOM images can be compressed as a regular JPEG lossy scheme (where some of the high-frequency information is lost) and without losses.

In medical imaging, they usually talk about the center of the window (window level, L) and the width of the window (window width, W) of the image. The window level is called some central value of the pixel intensities of the image. As a rule, by default, some average intensity value is set for the entire image dataset being processed. The width of the window allows you to set the range of pixel intensities of the image relative to the selected window level. All pixels whose intensity is less than the lower border of the selected window are assigned a zero value (black in the image), and all pixels whose intensity is greater than the upper border are assigned the maximum intensity (bright in the image). Selecting the width of the window allows you to stretch the tones of the image to the full range of brightness.

In magnetic resonance imaging, the contrast of images is relative and depends on the specific object under study and the type of image. Therefore, the selected level and width of the window, which is the best for one protocol, probably will not be suitable for another research protocol or another device.

The creation of a modern medical information system designed for several hundred automated workplaces is a multifaceted task, including:

- 1) building the necessary data transmission infrastructure;
- 2) purchase and installation of computer equipment and system software;
- 3) acquisition, modernization and development of application software;
- 4) training of personnel of computing centers;
- 5) ensuring the implementation of a medical information system;
- 6) maintenance and operation of the implemented system.

Medical images are divided into two main classes: linear images (for example, cardiograms), typical for functional diagnostics, and raster images (for example, radiographs), typical for radiation diagnostics. Linear images are often transmitted from the appropriate specialized system to the clinical information system. The transfer of raster images to the clinical information system is most often not practiced. To view and process such images, clinicians usually get the opportunity to directly connect via a computer network with a specialized system.

Currently, the complex processing of raster medical images is carried out by the systems of integration of radiation diagnostics (Computer Integrated Radiology SILD), which are integral components of the medical information system. Systems for archiving and transmitting medical images or PACS (Picture Archiving and Communication System) - refers to the technical implementation and is part of the SILD. SILD allows you to combine both intermediate and final research results into a single whole, allowing you to reconstruct 2D and 3D images and combine images obtained using different visualization devices.

The digital representation of images by modern diagnostic devices allows them to be integrated into the hospital computer network [8].

PACS system provides storage of a large amount of information, fast access, efficient processing of information.

Any PACS system consists of an image acquisition subsystem, a distributed database (archive server), a computer network for data transmission and workstations for image processing.

1.4 Methods of image analysis

One of the most informative modalities in the diagnosis of tumor is magnetic resonance imaging (MRI). An important feature of MRI is the ability to obtain images of an object with high spatial resolution and high tissue contrast. Due to the huge amount of imaging data obtained during clinical practice, researchers are paying special attention to the use of image analysis to improve existing standards for detecting tumors and gain a new understanding of the nature of the disease.

Currently, there are and apply various methods of analysis based on changing the brightness of pixels, separating the analyzed object, comparing and combining images, data reduction, contrast control. An example of such analysis methods: gradient method, segmentation method, clustering, etc.

1.4.1 Segmentation methods

Segmentation is a method of image analysis, the purpose of which is to separate the analyzed object, structure or area of interest from the surrounding background. Segmentation is an important tool in medical image processing, and it has been useful in many applications. Applications include detection of the coronary border on angiograms, quantitative assessment of multiple sclerosis lesion, surgery modeling, surgery planning, measurement of tumor volume and

its response to therapy, functional mapping, automatic classification of blood cells, study of brain development, detection of microcalcifications on mammograms, image registration, atlas comparison, heart analysis, extraction of images from cardioangiograms, detection of tumors, etc.

Segmentation methods can be divided into classes in different ways, depending on the classification scheme:

- manual, semi-automatic and automatic;
- pixel-based (local methods) and region-based (global methods);
- manual differentiation, low-level segmentation (threshold value, area magnification, etc.) and model-based segmentation (multispectral or spatial map methods, dynamic programming, contour tracking, etc.);
- classical (threshold, boundary and regional methods), static, fuzzy and neural network methods.

The most commonly used segmentation methods can be divided into two broad categories: (1) region segmentation methods that search for regions that meet a given uniformity criterion, and (2) boundary-based segmentation methods that search for boundaries between regions with different characteristics.

The thresholding method is a common method of segmentation of regions [9, 21]. In this method, a threshold is selected and the image is divided into groups of pixels whose values are less than the threshold value and groups of pixels whose values are greater than or equal to the threshold value [8,9]. There are several threshold value methods: global methods based on gray level histograms, global methods based on local properties, local threshold selection and dynamic threshold value. Clustering algorithms provide segmentation of the area [29, 30, 31, 32] by splitting the image into sets or clusters of pixels that have a strong similarity in the object space. The basic operation is to examine each pixel and assign it to the cluster that best represents the value of its characteristic vector of the objects of interest.

Region growing is another class of area segmentation algorithms that assign neighboring pixels or regions to the same segment if their image values are close enough, according to some pre-selected proximity criterion [33, 34].

The strategy of boundary-based segmentation algorithms is to find the boundaries of the object and segment the areas bounded by the boundaries [40, 37, 43, 35, 39, 44]. These algorithms usually work with edge magnitude and/or phase images created by an edge operator suitable for the expected image characteristics. For example, most gradient operators, such as the Pruitt, Kirsch, or Roberts operators, are based on the existence of an ideal stepped edge. Other edge-based segmentation methods are graph search and contour tracking [41, 36, 38].

Traditionally, most image segmentation methods use a single image type (MRI, CT, PET, SPECT, ultrasonography, etc.). However, the performance of these methods can be improved by combining images from multiple sources (multispectral segmentation [42]) or integrating images over time (dynamic or time segmentation [50]).

1.4.1.1 Threshold segmentation method

Several methods for determining threshold values have been developed [40, 49, 37, 43, 64, 44]. Some are based on the histogram of the image, others are based on local properties such as local mean and standard deviation or local gradient. The most intuitive approach is a global threshold value. The threshold method is called global if only one threshold is selected for the entire image based on the image histogram. If the threshold depends on the local properties of some areas of the image, for example, the local average value of the gray level of a pixel, the threshold value is called local. If local thresholds are selected independently for each pixel (or groups of pixels), the threshold value is called dynamic or adaptive.

Global threshold value

Global threshold processing is based on the assumption that the image has a bimodal histogram and, therefore, the object can be extracted from the background using a simple operation that compares the image values with the threshold value T [41]. Suppose we have an image $f(x,y)$ with the histogram shown in Figure 5.

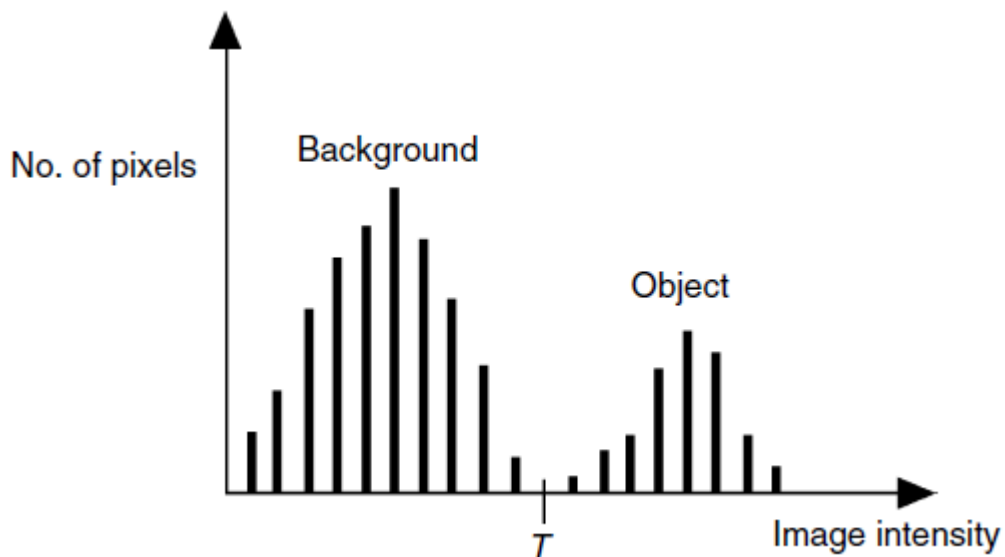


Figure 5 – Example of a bimodal histogram with a selected threshold T

The pixels of the object and background have gray levels grouped into two dominant modes. One of the obvious ways to highlight an object from the background is to select a threshold T separating these modes. The threshold image $g(x,y)$ is defined as

$$g(x,y) = \begin{cases} 1 & \text{if } (x,y) > T \\ 0 & \text{if } (x,y) \leq T \end{cases} \quad (4)$$

where $g(x,y)$ – threshold value;

T – threshold level.

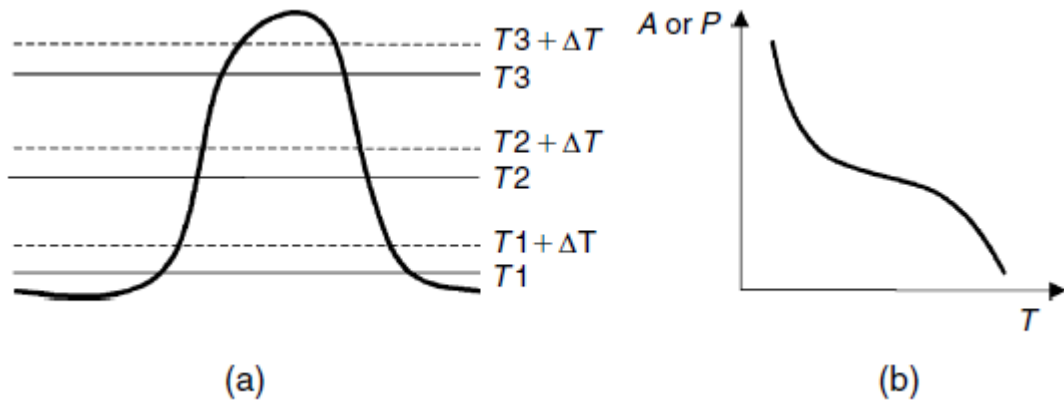
The result of threshold processing is a binary image, where pixels with an intensity value of 1 correspond to objects, and pixels with a value of 0 correspond to the background.

There are many other ways to choose a global threshold. One of them is based on a classification model that minimizes the probability of error [33]. For example, if we have an image with a bimodal histogram (for example, an object and a background), we can calculate the error as the total number of background pixels mistakenly classified as an object and object pixels mistakenly classified as a background.

A semi-automated version of this technique was applied by Johnson et al. [46] to measure ventricular volumes from 3D MRI-images. In their method, the operator selects two pixels - one inside the object and one in the background. When comparing the distribution of pixel intensities in circular areas around the selected pixels, a threshold value is automatically calculated and it corresponds to the smallest number of misclassified pixels between the two distributions.

The result of the threshold value operation is displayed as a contour map and superimposed on the original image.

If necessary, the operator can manually change any part of the border. The same method has also been applied to extract lymph nodes from CT scan images and has been found to be very sensitive to the user's placement of internal and external points.



(a) cross-sectional intensity profile of a bright object against a dark background with three threshold levels T1, T2 and T3 and three other levels obtained by adding a small value of ΔT; (b) Hypothetical plot of area (A) or perimeter (P) versus threshold T.

Figure 6 – Example of threshold selection sensitivity

In many applications, appropriate segmentation is achieved when the area or perimeter of objects is minimally sensitive to small changes in the selected threshold level. Figure 6a shows the intensity profile of an object that is brighter than the background and three threshold levels for segmentation: T1, T2 and T3. A small change in ΔT at the lowest threshold level will result in a significant change in the area or perimeter of the segmented object. The same is true for the highest threshold level. However, a change in ΔT at an average level will have a minimal effect on the area or perimeter of the object. The area of the object A(T) and the perimeter P(T) are functions of the threshold T, which often show the trend shown in Figure 6b.

Therefore, a threshold level that minimizes either $dA(T)/dT$ or $dP(T)/dT$ is often a good choice, especially in the absence of operator guidance and when prior information about the object's location is not available.

The average value of the gradient is determined by the formula

$$\bar{G} = \lim_{\Delta T \rightarrow 0} \frac{\Delta T \times P(T)}{\Delta A} = \frac{P(T)}{H(T)} \quad (5)$$

where H(T) – function of histogram. A threshold value is selected that maximizes the average boundary gradient;

P(T) – perimeter of object;

ΔA– area change;

ΔT– threshold change.

If an image contains more than two types of regions, it can still be segmented by applying several separate thresholds [44] or using the multitasking method [47].

As the number of areas increases, the histogram modes become more difficult to distinguish, and the selection of the threshold becomes more difficult.

The global threshold value is simple and fast to calculate. It works well on images containing objects with the same intensity values on a contrasting background. However, it fails if there is low contrast between the object and the background, if the image is noisy, or the background intensity varies significantly all over the image.

Local (Adaptive) Threshold

In many applications, the global threshold cannot be found from the histogram, or a single threshold cannot give good segmentation results across the entire image. For example, when the background is not constant and the contrast of objects varies throughout the image, thresholding may work well in one part of the image, but may not work well in other areas. If background changes can be described by some known position function in the image, one can try to correct this using gray level correction methods, after which a single threshold should work for the entire image. Another solution is to use a local (adaptive) threshold [41, 49, 43].

Local thresholds can be determined by: (1) dividing the image into sub-images and calculating threshold values for each sub-image, or by (2) examining the intensity of the image in the vicinity of each pixel. In the first method [48], the image is first divided into rectangular overlapping image fragments, and histograms are calculated for each image fragment. The image fragments used must be large enough to include both object and background pixels. If the image fragment has a bimodal histogram, then the minimum between the peaks of the histogram should determine the local threshold. If the histogram is unimodal, the threshold can be assigned by interpolating from the local threshold values found for the nearest image fragments. At the last stage, a second interpolation is needed to find the correct thresholds for each pixel.

In the latter method, the threshold can be chosen using the average value of the local intensity distribution. Sometimes other statistics data can be used, such as the mean value plus the standard deviation, the average value of the maximum and minimum values [40, 49] or statistics based on the magnitude of the local intensity gradient [49].

1.4.1.2 Region growing method

Region growing method is a contextual form of segmentation that takes into account the distance of pixels to the current area. Region growth algorithms are considered classical methods that form the basis for complex permutations of region growing methods.

While the threshold method focuses on the difference in pixel intensities, the region growth method looks for groups of pixels with the same intensity. Region growth, also called region pooling, starts with a pixel or group of pixels (called seeds) that belong to the structure of interest. Seeds can be selected by the operator or provided through an automatic seed search procedure. In the next step, neighboring pixels are tested one at a time and added to the growth area if they are sufficiently similar based on a uniformity test (also called a uniformity criterion). The procedure continues until the pixels stop being added. Then the object is represented by all the pixels that were taken during the zoom procedure.

One example of a uniformity test is to compare the difference between the pixel intensity value and the average intensity value an area. If the difference is less than a given value, for example, two standard deviations of intensity over the entire area, then the pixel is included in the area, otherwise it is defined as a boundary pixel.

The results of the method strongly depend on the choice of the uniformity criterion. If it is not selected correctly, the areas leak into adjacent areas or merge with areas that do not belong to the object of interest. Another problem with the method of growing regions is that different starting points may not turn into the same regions. The advantage of the region growth method is that they are able to correctly segment areas that have the same properties. Another advantage is that it generates connected regions.

Instead of combining regions, can start with some initial segmentation and divide the regions that do not meet the specified uniformity criterion. This method is called splitting [43, 44]. The combination of separation and fusion combines the advantages of both approaches [41].

Various approaches to segmentation of the growing region were described by Zucker [70]. Excellent reviews of regional cultivation methods were made by Fu and Mui [71], Haralik and Shapiro [43], as well as Rosenfeld and Kak [44].

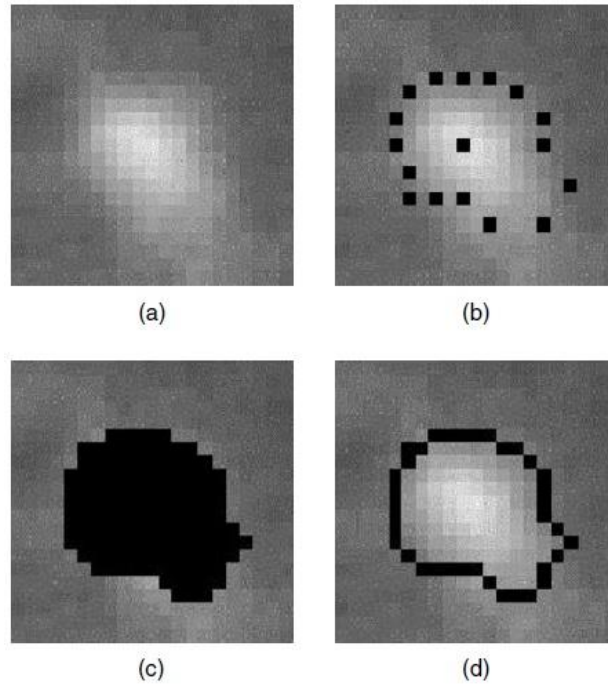
An interesting modification of the region growth technique called hill climbing was proposed by Bankman et al. to detect microcalcifications on mammograms [14]. This method is based on the fact that in a given image $f(x, y)$, the microcalcification edge to be segmented is a closed loop around a known pixel (x_0, y_0) , a local intensity maximum. For each pixel, the slope value $s(x, y)$ is defined as

$$s(x, y) = \frac{f(x_0, y_0) - f(x, y)}{d(x_0, y_0, x, y)}, \quad (6)$$

where $d(x_0, y_0, x, y)$ —Euclidean distance between the local maximum pixel and the (x, y) pixel;

$f(x, y)$ — image;

$f(x_0, y_0)$ —image of the selected object.



(a) 0.5×0.5 mm image showing fine microcalcifications; (b) 16 edge points determined by the algorithm, (c) the result of the growth of the area; (g) the edges of the area covering the segmented microcalcification[14].

Figure 7 – Segmentation stages using the hill climbing algorithm

At the first stage, the edge points of the object are identified by searching for a radial line originating from the local maximum. Linear search is applied in 16 equally spaced directions emanating from the pixel (x_0, y_0) , and for each direction, the pixel is considered to be on the edge if it provides the maximum slope value. Then the edge points are used as starting points for the growth of the area with a spatial restriction (the growth of the area inward, to the local maximum) and intensity restriction (including pixels with intensity values monotonically increasing to the local maximum). Figure 7 shows the segmentation stages using the hill climbing algorithm. The advantages of this algorithm are that it does not require the selection of a threshold and, since it increases the area from the edges to the center, it avoids excessive growth of the area.

The increase in the area has found many other medical applications, such as segmentation of the ventricles in images of the heart, extraction of blood vessels according to angiography, segmentation of the kidneys or extraction of the brain surface [36].

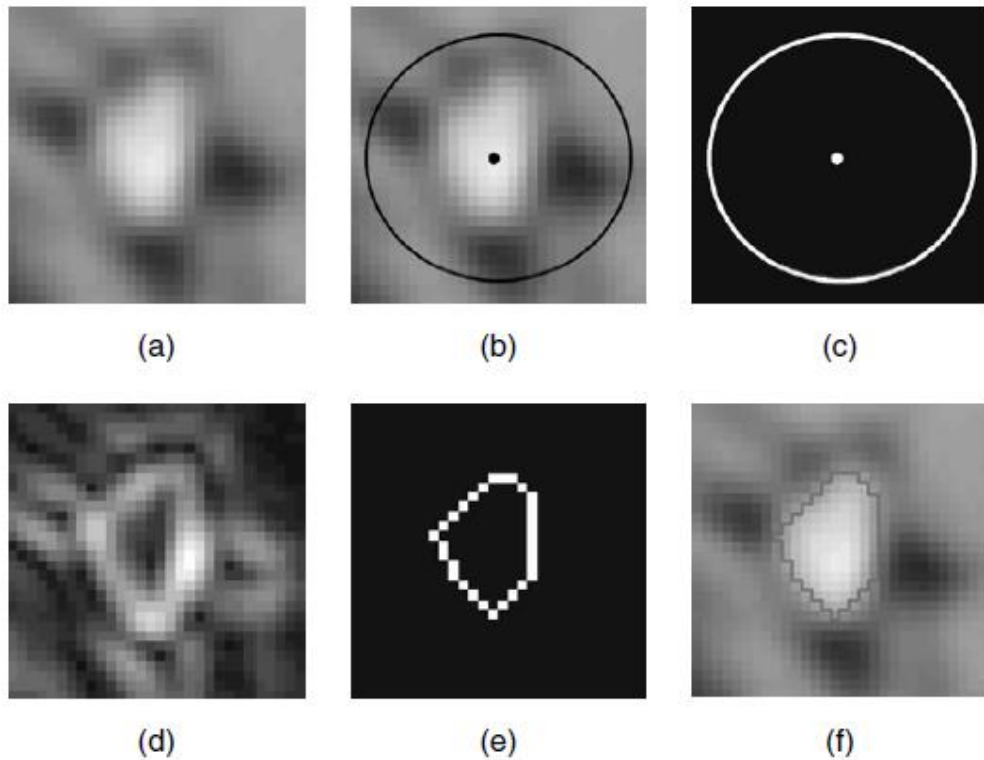
1.4.1.3 Watershed method

The watershed method is a regional method using image morphology. This requires selecting at least one marker (the "starting" point) inside each image object, including the background as a separate object. Markers are selected by the operator or provided using an automatic procedure that takes into account the knowledge of objects specific to a particular application. Once the objects are marked, they can be grown using morphological transformation of the watershed [40].

To understand the watershed, can be think of an image as a surface where bright pixels represent mountain peaks and dark pixels represent valleys. The surface is pierced in some valleys, and then slowly immersed in a water bath. Water will pour into each puncture and begin to fill the depressions. However, water from different punctures is not allowed to mix, and therefore dams must be built in places of first contact.

These dams are the boundaries of water basins, as well as the boundaries of image objects.

The use of watershed segmentation to isolate lymph nodes in computed tomography images is shown in Figure 8. In this implementation, the Sobel edge operator 3×3 [37, 44] is used instead of a morphological gradient to extract the edge strength.



(a) The original image of the lymph node; (b) operator marks: a point inside a node and a circle enclosing an area well outside the node; (c) a binary image generated from (b); (d) the result of a 3×3 Sobel edge detection operation performed on the original image (a); (e) the result of a watershed algorithm performed on image (d) using markers from image (c); (f) the edges of the lymph node [inner area from the image (e)] superimposed on the original image[74].

Figure 8 – Image segmentation using the Sobel algorithm/watershed

The original image of the lymph node is shown in Figure 8a. In the first step, the operator places the cursor inside the node in Figure 8b. All pixels within a two-pixel radius of the placemark are used as starting points for the lymph node. To mark the outer part of the lymph node, the operator moves the cursor outside the node to define a circular area that completely covers the node in Figure 8c. All pixels outside of this circle represent the background.

In the next step, the edge image is created using the Sobel operator (Figure 8d). An edged image has high values for pixels with sharp edges. With a starting point denoting the inside of the node, a circle denoting the background, Figure 8c, and an edge image generated by the Sobel operator, Figure 8d, segmentation is performed directly using the watershed operation, Figure 8e. The "Watershed" operation is performed on the edge image to separate the lymph node from the surrounding tissue.

Using a technique called immersion simulation [75], the watershed takes into account whether a drop of water at each point of the edge image will flow to the inner starting point or to

the outer marker. The points that drain inwards belong to the lymph node, while the points that drain outwards belong to the surrounding tissue.

Watershed analysis has proven to be a powerful tool for many applications of 2D image segmentation [52].

Higgins and Ojard [51] applied a 3D extension of the watershed algorithm to 3D cardiac images. Grau et al. combined watershed transformation and atlas registration using markers and applied this technique to knee cartilage and gray matter/white matter segmentation in MR-images [55]. Marker-controlled watershed segmentation has also been successfully applied to detect lymph nodes on CT-images [54]. Gulsrud et al. used the watershed method to segment detected lesions on digital mammograms [52].

1.4.2 Methods for selecting the boundaries of object

The edge or border of an image is defined by a local pixel intensity gradient. A gradient is an approximation of the first order derivative of an image function. For a given image $f(x, y)$ we can compute the magnitude of the gradient as

$$|G| = \sqrt{[G_x^2 + G_y^2]} = \sqrt{\left[\left(\frac{\partial f}{\partial x}\right)^2 + \left(\frac{\partial f}{\partial y}\right)^2\right]}, \quad (7)$$

where G_x —gradient in x direction;

G_y — gradient in y direction.

and the direction of the gradient in the form

$$D = \tan^{-1}\left(\frac{G_x}{G_y}\right), \quad (8)$$

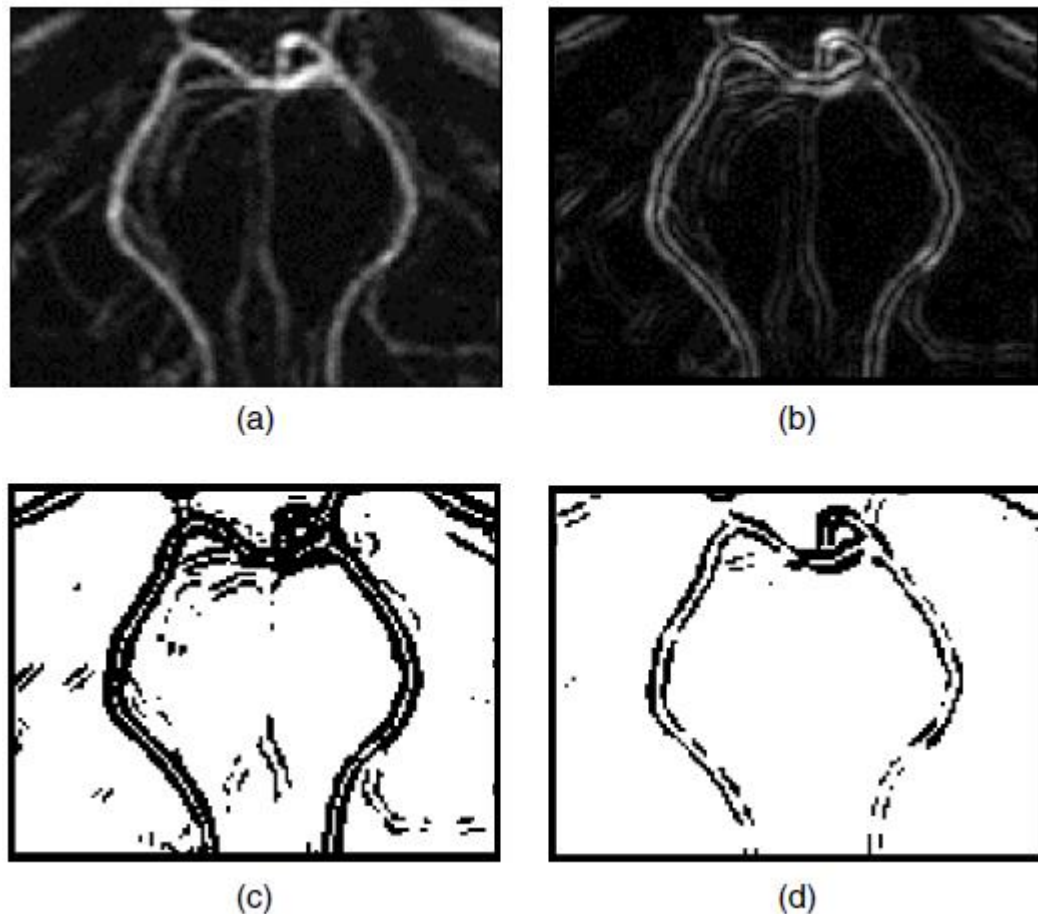
where G_x —gradient in x direction;

G_y — gradient in y direction.

Since the discrete nature of digital images does not allow for the direct application of continuous differentiation, the gradient calculation is performed by differentiation [37].

The magnitude image will have gray levels that are proportional to the magnitude of the local intensity changes, while the direction image will have gray levels representing the direction

of the maximum local gradient in the original image. Most gradient operators in digital images involve the calculation of convolution, for example, weighted summation of pixel intensities in local neighborhoods. Weights can be listed as a numeric array in a form corresponding to the local neighborhood of the image (also known as a mask, window, or kernel).



(a) An initial angiographic image showing blood vessels, (b) an image of the edge size obtained using a 3×3 Sobel mask, (c) an image of an edge with a threshold value with a low threshold ($T = 300$), (d) an image of an edge with a threshold value with a high threshold ($T = 600$) [53,76].

Figure 9 – Defining boundaries using the Sobel operator.

An image of the gradient magnitude is generated by combining G_x and G_y using Equation 7. Figure 9b shows an image of the edge magnitude obtained using the 3×3 Sobel operator applied to the magnetic resonance angiography (MRA) image in Figure 9a.

The results of edge detection depend on the gradient mask. Some of the other border operators are Roberts, Pruitt, Robinson, Kirsch and Freichen [37, 43, 44].

Many edge detection methods use a gradient operator followed by a threshold operation on the gradient to determine if an edge has been found [50, 48, 49, 43, 57, 53, 44]. As a result, the output is a binary image indicating where the edges are. Figures 9c and 9d show the results of the threshold value at two different levels.

A combination of vertical gradient and Sobel edge detection with adaptive filtering was used by Rogowska et al. to detect cartilage edges in optical coherence tomography images [53].

Edge-based methods are computationally fast and do not require a priori information about the image content. A common problem with edge-based segmentation is that often the edges do not cover the object completely. To form closed boundaries surrounding the regions, a post-processing stage is required for linking or grouping edges that correspond to a single boundary. The simplest approach to edge binding involves examining pixels in a small neighborhood of an edge pixel (3×3 , 5×5 , etc.) and associating pixels with a similar edge size and/or edge direction. In general, binding boundaries is computationally expensive and not very reliable. One solution is to make edge snapping semi-automatic and allow the user to draw edges when the automatic tracing becomes ambiguous. For example, Wang et al. We have developed a hybrid algorithm (for MR-syneangiography of the heart) in which a human operator interacts with the edge tracing operation, using anatomical knowledge to correct errors [56].

The graph search method for detecting boundaries has been used in many medical applications [41, 36, 39, 38]. In this method, each pixel of the image corresponds to a node of the graph, and each path in the graph corresponds to a possible edge of the image. Each node has a cost associated with it, which is usually calculated using the magnitude of the local edge, the direction of the edge, and a priori knowledge of the shape or location of the boundary.

The cost of a graph path is the sum of the costs of all nodes included in the path. By finding the optimal inexpensive path on the graph, possible determine the optimal boundary.

The graph search method is very powerful, but it strongly depends on the cost function specific to a particular application.

Since the peaks in the first-order derivative correspond to zeros in the second-order derivative, the Laplace operator (which approximates the second-order derivative) can also be used to detect edges [40, 37, 44].

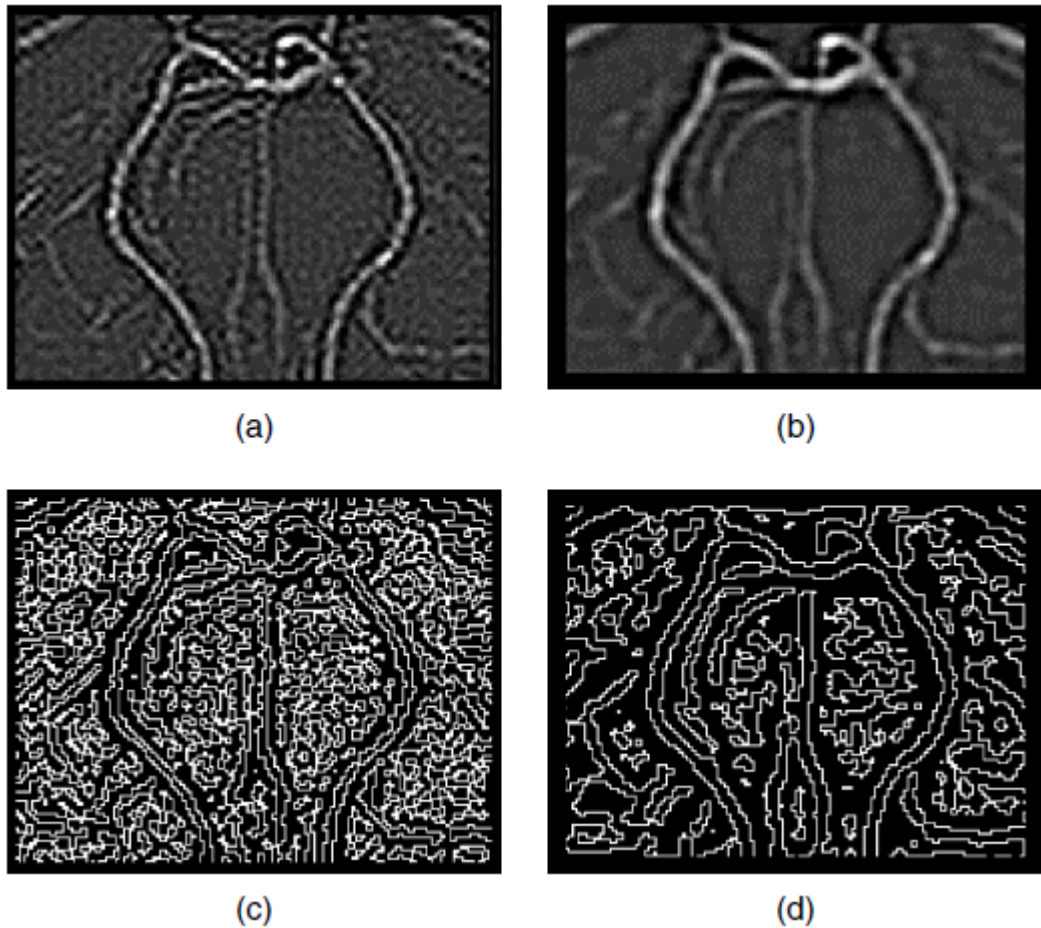
The Laplace operator ∇^2 of the function $f(x,y)$ is defined as

$$\nabla^2 f(x,y) = \frac{\partial^2 f(x,y)}{\partial x^2} + \frac{\partial^2 f(x,y)}{\partial y^2}; \quad (9)$$

where ∇^2 –Laplace operator;

$f(x,y)$ –image.

Laplace is approximated in digital images by the convolution mask N by N [44].



(a) a 3×3 Laplace image, (b) a 7×7 Gaussian smoothing result followed by a 7×7 Laplacian, (c) a zero crossing of the Laplacian image (a), (d) zeroing of the log image (b)[57].

Figure 10 – Results of the Laplace and Laplace-Gauss operator applied to the original image shown in Figure 9a

The edges of the image can be found by finding pixels in which the Laplacian makes a transition through zero (zero intersections). Figure 10a shows the result of calculating the 3×3 Laplacian applied to the image in Figure 9a. The zero intersections of the Laplacian are shown in Figure 10c. All boundary detection methods based on gradient or Laplacian are very sensitive to noise. In some applications, noise effects can be reduced by smoothing the image before applying the crop operation. Mar and Hildreth [57] proposed smoothing the image using a Gaussian filter before applying the Laplacian (this operation is called the Gaussian Laplacian, Log).

Figure 10b shows the result of a 7×7 Gaussian followed by a 7×7 Laplacian applied to the original image in Figure 9a. The intersections of the zeros of the registration operator are shown in Figure 10d.

1.4.3 Multispectral methods

Most traditional segmentation methods use images that represent only one type of data, such as MRI or CT. If different images of the same object are obtained using multiple imaging techniques, such as CT, MRI, PET, ultrasonography, or image acquisition over time, they can provide different characteristics of the objects, and this spectrum of features can be used for segmentation.

Segmentation methods based on combining information from several images are called multispectral or multimodal [58, 42].

Segmentation using multiple Images obtained using different Visualization Methods

In the case of a single image, pixel classification is based on a single object (gray level), and segmentation is performed in a one-dimensional (single-channel) object space. In multispectral images, each pixel is characterized by a set of features, and segmentation can be performed in a multidimensional (multichannel) feature space using clustering algorithms. For example, if MR-images were collected using T1, T2 and a proton density imaging protocol, a relative multispectral data set for each class of tissues leads to the formation of tissue clusters in the three-dimensional space of objects. The simplest approach is to construct a 3D scattering diagram, where the three axes represent pixel intensities for images T1, T2 and proton densities. Clusters on such a scattering diagram can be analyzed, and segmentation rules for different tissues can be determined using automatic or semi-automatic methods [58].

There are many segmentation methods used in multimodal images. Some of them are k-nearest neighbors (kNN) [60], k-means [72], fuzzy c-means [50], artificial network algorithms [59], mathematical expectation/maximization [61] and adaptive template moderated spatially varying statistical classification methods [62]. All multispectral methods require proper image registration. To reduce noise and improve the performance of segmentation methods, images can be smoothed. Excellent results were obtained using adaptive filtering, such as Bayesian processing, nonlinear anisotropic diffusion filtering and filtering using wavelet transformations [63].

Adaptive segmentation is a generalization of the standard intensity-based classification, which, in addition to the usual models of conditional intensity of a class of tissues, includes models of inhomogeneities of intra- and interscanning intensity that usually occur in images. The algorithm is an iterative algorithm that alternates the traditional statistical classification of tissues (step "E") and the re-evaluation of the correction for unknown intensity heterogeneity (step "M").

The "E", "M" approach can be motivated by the following observations. If an improved intensity correction is available, it is simple to apply it to the intensity data and get an improved classification. Similarly, if an improved classification is available, it can be used to obtain an improved intensity correction, for example, by predicting the intensity of an image based on a tissue class, comparing predicted intensities with observed intensities, and smoothing. Eventually, the process converges, usually in less than 20 iterations, and gives classification and intensity correction.

The algorithm "E", "M" has been expanded in a number of ways. Spline-based modeling of intensity artifacts associated with surface coils has been described by Gilles et al. [44]. The addition of an "unknown" class of fabrics and other improvements were described by Guillemaud and Brady [64].

In addition, Markov models of tissue uniformity were added to the formalism to reduce thermal noise, which is usually manifested in MRI-images. Held et al. [60] used the method of iterative conditional modes to solve the resulting combinatorial optimization problem, while Kapoor et al. [65] used mean field methods to solve the related continuous optimization problem.

Segmentation using multiple images obtained over time

Multispectral images can also be obtained as a sequence of images in which the intensity of certain objects changes over time, but the anatomical structures remain stationary. One example of such a sequence is a series of computed tomography images obtained after intravenous injection of a contrast agent that is transferred to the organ of interest. Such a sequence of images has a constant morphology of the depicted structure, but regional intensity values may vary from one image to another depending on the local pharmacokinetics of the contrast agent.

The most popular segmentation method using both intensity information and temporal information contained in image sequences is the parametric analysis method [66].

In this method, for each pixel or area of interest, the intensity is displayed depending on the time. Next, the graphs are analyzed under the assumption that the curves have similar time characteristics.

Certain parameters are selected, such as the maximum or minimum intensity, the distance between the maximum and minimum, or the time of occurrence of the maximum or minimum. The corresponding set of parameters depends on the functional characteristics of the object under study. Then an image is calculated for each of the selected parameters. In such images, the value of each pixel is made equal to the value of the parameter at this point.

Therefore, this method is called parametric visualization. The disadvantage of the parametric analysis method is that it assumes that all pixel intensity sequence graphs have the

same general pattern throughout the image. In fact, however, many images have pixels or regions of pixels that do not have the same characteristics in the time domain and therefore will have different dynamic intensity graphs.

An interesting application of the parametric mapping method for 3D segmentation of multiple sclerosis foci on a series of MRI-images was proposed by Gerig et al. [67]. Temporary images were obtained at intervals of 1, 2 or 4 weeks for 1 year. The parameters selected for parametric maps were based on the characteristics of the lesion, such as the dispersion of the intensity of the lesion, the time of appearance and the time of disappearance.

3D maps showed samples of lesions that demonstrate similar temporal dynamics. Another method of time segmentation was introduced by Rogowska [68]. The correlation mapping method (also called similarity mapping) identifies regions (or objects) according to their temporal similarity or difference with respect to the reference time intensity curve obtained from the reference area of interest (ROI). Suppose we have a sequence of N spatially recorded temporal images of stationary structures. The $NCOR_{ij}$ similarity map based on normalized correlation is defined for each pixel (i,j) as

$$NCOR_{ij} = \frac{\sum_{n=1}^N (A_{ij}[n] - \mu_A) (R[n] - \mu_R)}{\sqrt{\sum_{n=1}^N (A_{ij}[n] - \mu_A)^2 \sum_{n=1}^N (R[n] - \mu_R)^2}}, \quad (10)$$

where $A_{ij}[n]$ – time sequence of image intensity values for consecutive N images: $A_{ij}[1], A_{ij}[2], \dots, A_{ij}[N]$, ($i = 1, 2, \dots, I, j = 1, 2, \dots, J, n = 1, 2, \dots, N$;

I –number of image lines;

J –number of image columns;

$R[n]$ –reference sequence of average intensity values from the selected reference ROI;

μ_A –the average value of the time sequence for pixel (i,j);

μ_R –the average value of the reference sequence.

Pixels on the resulting similarity map, whose time sequence is similar to the reference one, have high correlation values and are bright, while pixels with low correlation values are dark. Thus, similarity mapping segments structures in a sequence of images based on their temporal characteristics rather than spatial properties. In addition, similarity maps can be displayed in pseudo-color or color coding and superimposed on a single image.

Other researchers have used this method in studies of brain activation [69], segmentation of breast tumors [50] and kidney pathologies.

A modification of the correlation mapping method, called delay mapping, is also used to segment time sequences of images. It segments the image into areas with different time delays, which are calculated relative to the reference.

Parametric maps, similarity maps, and delay maps are all tools for segmentation and visualization of time sequences of images. They are especially useful for evaluating disease processes, drug treatment, or the results of radiation therapy.

1.4.4 Clustering

Clustering is the organization of data with high intracluster similarity and low intercluster similarity. To find the similarity or dissimilarity between two data points, that is, the distance between the pixels of the image is calculated. This distance can be the brightness difference between two pixels. The most commonly used clustering methods are: k-means [24].

The clustering method means splitting an image into separate areas in order to determine the textures on these images. Cluster analysis is a set of mathematical methods designed to form groups of objects that are relatively distant from each other based on information about distances or connections between them.

The most common clustering algorithm is k-means. This method is an iterative method for splitting an image into k number of clusters, and each cluster has a distinct, unknown intensity value, called the average value of the cluster, denoted by μ_i , $i=1, \dots, k$. The action of the algorithm is such that it seeks to minimize the total quadratic deviation of cluster points from the centers of these clusters [25]:

$$\min \left[\sum_{i=1}^k \sum_{x \in S_i} (x - \mu_i)^2 \right], \quad (11)$$

where k – number of clusters;

S_i – the resulting clusters;

μ_i – cluster centers, $i=1, \dots, k$.

2 Material and methods

2.1 Principal component analysis

The Principal component analysis (PCA) is a basic approach used in chemometrics to solve a variety of problems, one of the ways to reduce the dimension of data by losing the least amount of data. It is used in the fields of econometrics, bioinformatics, image processing, for data compression in the social sciences [45].

The principal component analysis is applied to data written in the form of an X matrix with dimensions of I rows and J columns. The rows of the matrix are called samples and numbered by index $i=1,\dots,I$. The columns are called variables and numbered by index $j=1,\dots,J$.

The goal of the PCA is to:

- extracting the most important information;
- reducing the size of the data set by saving the necessary information.

To achieve these goals, the original matrix is replaced by two new matrices T and P, the dimension of which, A, is less than the number of variables J in the original matrix.

The second dimension - the number of samples I is preserved. If the decomposition is done correctly - the dimension of the matrices, A, is chosen correctly, then the matrix T carries as much information as it had at the beginning, in the original matrix.

Formal description

The principal component analysis uses new, formal variables $t_a(a=1,\dots,A)$, which are a linear combination of the original variables $x_j(j=1,\dots,J)$

$$t_a = p_{a1}x_1 + \dots + p_{aj}x_j, \quad (12)$$

where t_a – new variables;

$p_{aj}x_j$ – source variables;

$$X = TP^t + E = \sum_{a=1}^A t_a p_a^t + E, \quad (13)$$

where T – matrix of accounts with dimension (IxA);

P – load matrix with dimension (JxA);

E – matrix of residuals with dimension (IxJ).

The new variables t_a are called the principal components. The number of columns t_a in the matrix T , and p_a in the matrix P , is equal to A , which is called the number of principal components.

An important property of the principal component method is the orthogonality (independence) of the principal components.

To build a PCA of accounts and loads, a recurrent algorithm is more often used - Nipals [79], which calculates one component at each step. By the first action, the original matrix X is transformed and transformed into the matrix E_0 , $a = 0$. The second action is the application of the algorithm:

1. choosing the initial vector t ;
2. $p^t = t^t E_a / t^t t$;
3. $p = p / (p^t p)^{1/2}$;
4. $t = E_a p / p^t p$.

After calculating the (a-th) components, it is assumed that $t_a = t$ and $p_a = p$. To calculate the following components, it is necessary to calculate the residuals $E_{a+1} = E_a - t p^t$ and apply the same algorithm, while replacing the index a with $a+1$.

2.2 Classification of MRI data for two pathologies

In my work, I used a sample of 2 groups. Each group consisted of 100 patients, each in turn containing 3 .dicom images. MRI-images were obtained in FLAIR scanning mode. Pathologies: glioblastoma and astrocytoma [9, 78].

The collection of data that I used in my work is licensed under the Creative Commons Attribution 3.0 license and is freely available on the Internet (<https://creativecommons.org/licenses/by/3.0/>). Creative Commons is a global non-profit organization that promotes the sharing and reuse of creativity and knowledge through the provision of free legal tools.

It allows you to freely:

- Share (exchange) - copy and distribute material on any medium and in any format;
- Adapt (create derivative materials) - remix, modify and create new, based on this material for any purpose, including commercial.

if the following conditions are met:

1. Attribution - The user must provide appropriate attribution, provide a link to the license, and indicate changes, if any, have been made. This can be done in any reasonable way, but not in a way that implies that the licensor approves of you or your use of the work;

2. No Additional Restrictions - The User may not impose legal restrictions or technological measures that create legal barriers for others to do anything that is permitted by the license.

FLAIR scan mode

FLAIR is another variation of the inversion-recovery sequence. In the FLAIR sequence, the liquid signal is canceled out by using a long TE echo time and a long TI. An inversion-recovery sequence with a long inversion time (TI) of 2000-2500ms is used for liquid suppression. In FLAIR imaging, CSF (cerebrospinal fluid) and other fluids in the brain or spinal cord appear dark, causing lesions or other pathological processes to appear bright.

Astrocytoma is a tumor that develops from the astrocytic part of the glia and is represented by astrocytes. It can be localized both in the cerebral hemispheres and in the cerebellum, as well as in the brain stem and spinal cord. There are low (Grade I–II) and high (Grade III–IV) grade astrocytomas[73].

Glioblastoma is a tumor that develops from glial cells of the nervous tissue of the brain. An extremely aggressive tumor classified as high grade Grade IV[73].

The support vector machine (SVM) is a set of similar supervised learning algorithms used for classification and regression analysis problems. The property of the method is a continuous decrease in the empirical classification error and an increase in the gap. The main idea of the method is to translate the original vectors into a higher-dimensional space and search for a separating hyperplane with the largest gap in this space [77].

3 Development of approaches for the analysis of MRI data and their classifications

This chapter analyzes brain MRI-images for the following pathologies: glioblastoma and astrocytoma.

Images were searched from different sources with the same license. 300 glioblastoma images and 300 astrocytoma images were found. Figure 11 shows an example of MRI-images of the brain with pathologies: a) glioblastoma, b) astrocytoma.

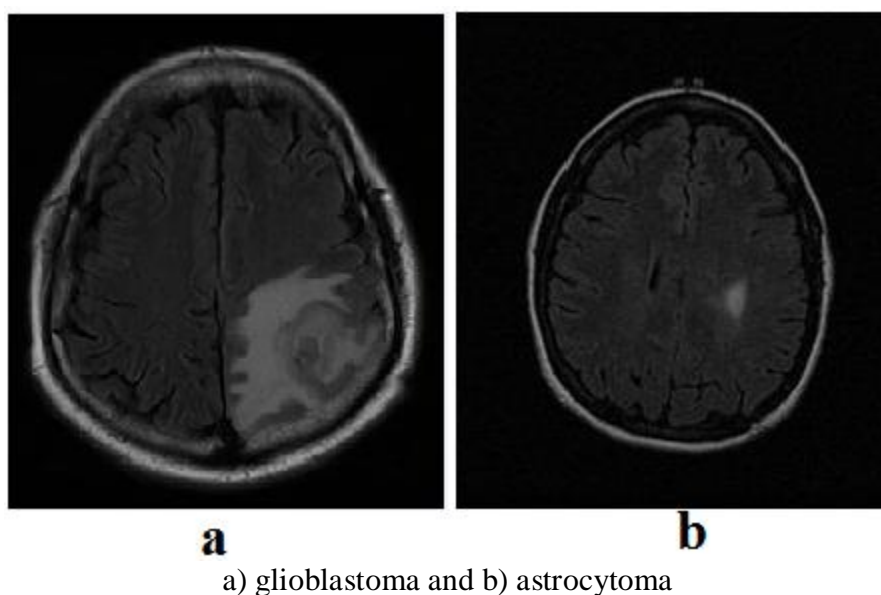


Figure 11 –MRI-image of the human brain

The difference between pathologies lies in their degree of malignancy. In Figure 11b, it can be seen that the degree of focal lesions is lower compared to Figure 11a. But if we take into account the astrocytoma with a high degree of focal lesions, then it is not possible to distinguish visually. This requires the development of a classification program.

The dataset was converted from .dicom format to raster graphics format .jpg or .png. This was done by a separate program, shown in Figure 12.

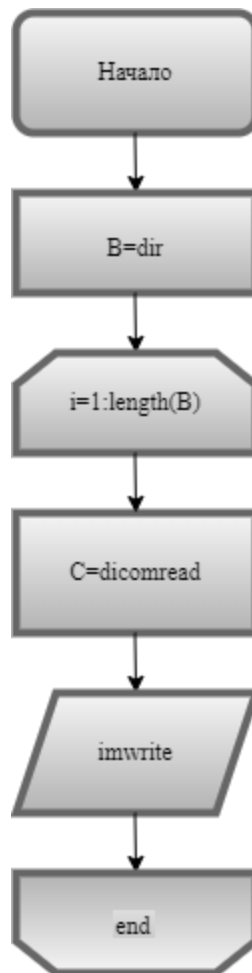
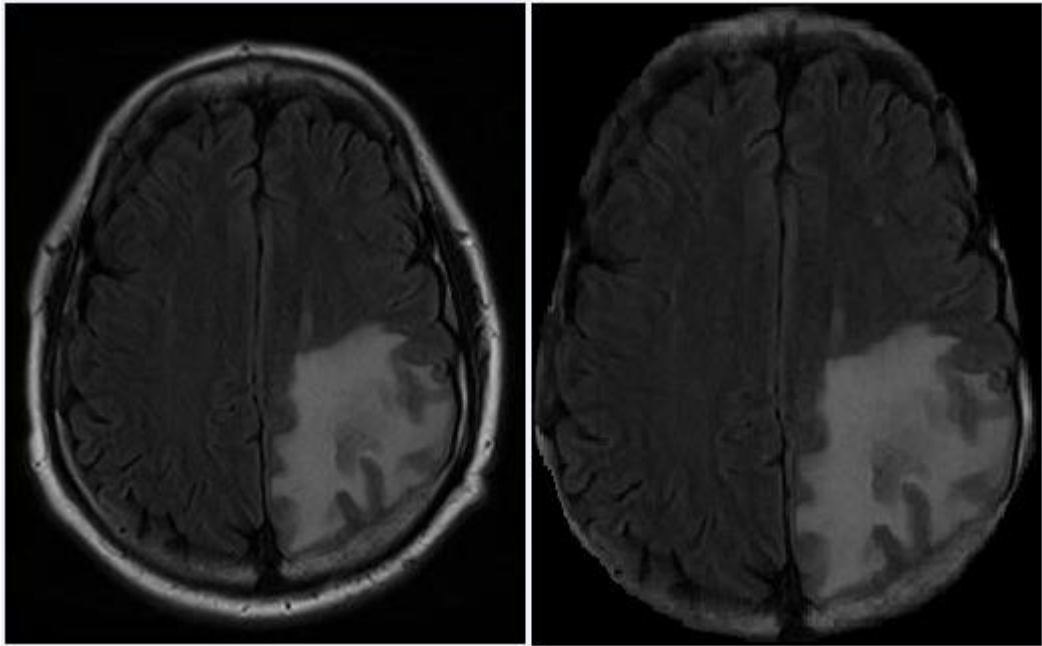


Figure 12 – Flowchart of the general workflow of converting images

After translating the data set, the next step was to separate the bone structure (structure of the skull) from the brain, using the PAINT bitmap graphics editor, using the "Select" tool. The separation was carried out to reduce the objects for analysis. Figure 13 shows an MRI image a) with bone structure and b) without bone structure.



(a) original image, (b) image without bone structure.

Figure 13 – Removal of bone from brain structure

The resizing of the images was carried out by the program indicated in Figure 14.

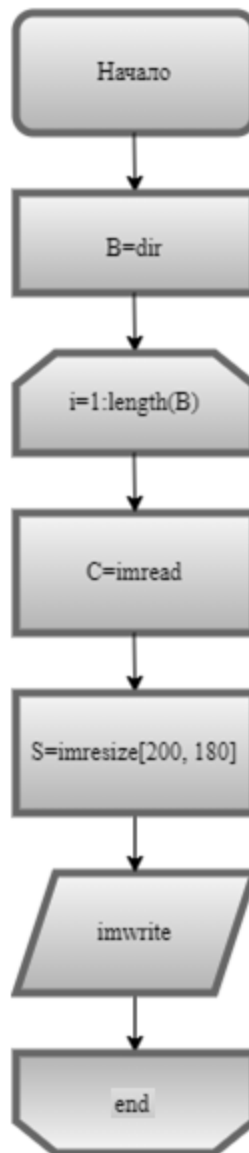


Figure 14 – Flowchart of a general workflow for image dimensionality reduction

The analysis and classification of MRI-images was carried out by the program shown in Figure 15. The program algorithm consists of the following steps:

- 1) Reading images;
- 2) Application of the Canny operator;
- 3) Application of the threshold method;
- 4) Calculation of probability according to the formula:

$$P_i = \frac{N_i}{N},$$

where N_i – the number of pixels in the i -th interval;
 N – the total number of pixels.

- 5) Calculation of the average probability and standard deviation:

$$P_{cp} = \frac{\sum P_i}{N},$$

where P_i —probability;

N —the total number.

$$\sigma = \sqrt{\frac{\sum (P_i - P_{cp})^2}{N - 1}},$$

where P_i —probability;

P_{cp} —average probability;

N —the total number.

- 6) Application of the principal component method;
7) Application of the support vector machine.

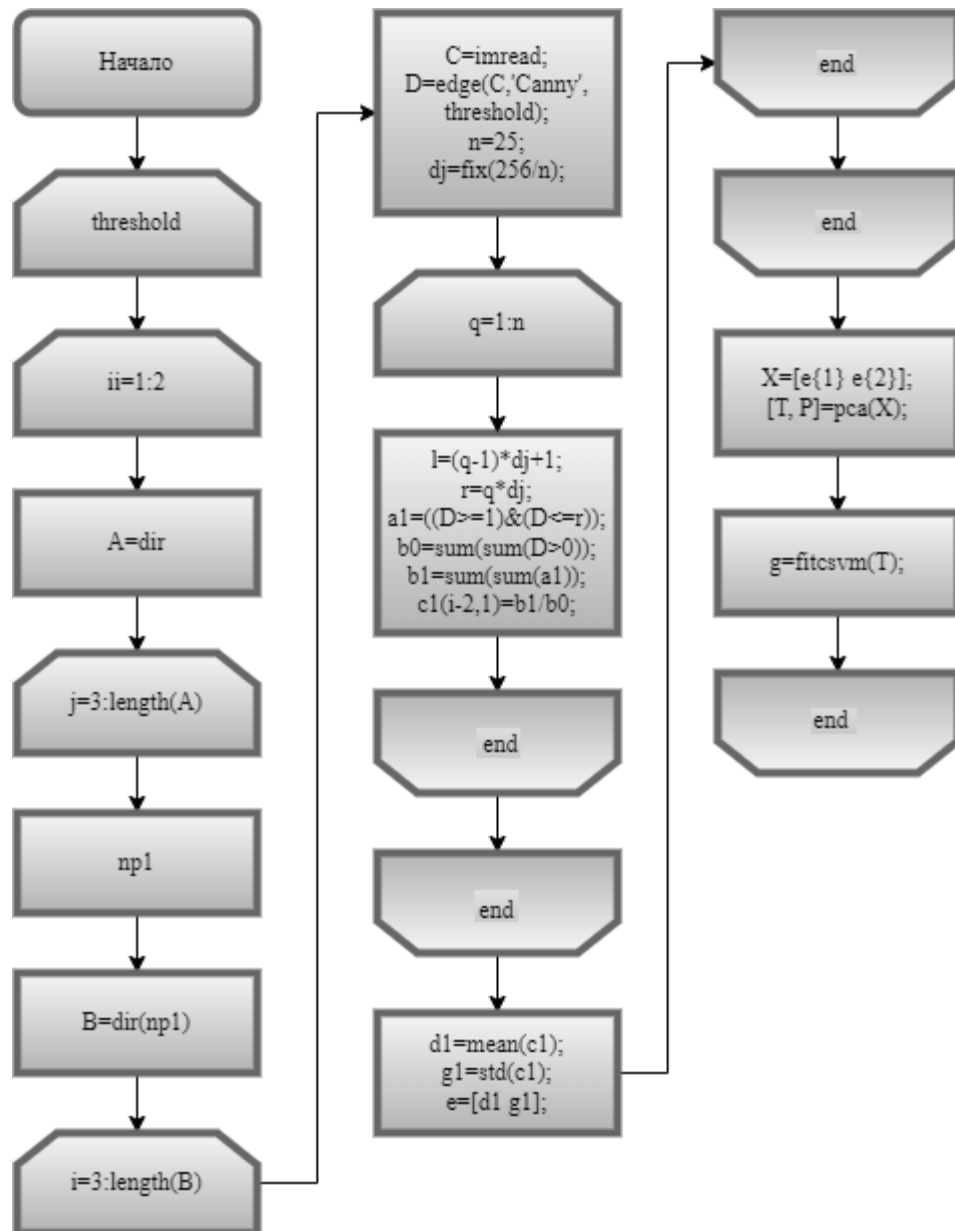


Figure 15 – flowchart of the general workflow for the MRI image analysis and classification program

The values for the thresholding method were taken in the range from 1 to 250, with a step of 10. The threshold value of the Canny operator was taken in the range from 0.1 to 0.9, with a step of 0.1 and a filter standard deviation of 0.1. The result of using the support vector machine is shown in Table 1.

Table 1 – Result of support vector machines using the Canny operator

Canny operator threshold value	Classified, %	
	Glioblastoma	Astrocytoma
0.1	0	100
0.2	3	96
0.3	3	96
0.4	3	96
0.5	3	96
0.6	0	100
0.7	3	96
0.8	3	96
0.9	0	100

For comparison, a similar action was carried out without the Canny operator. As a result, the maximum value of the similarity of the pathology of glioblastoma was 0%, astrocytoma – 93%.

The result of the principal vector method is shown in Figures 16–21.

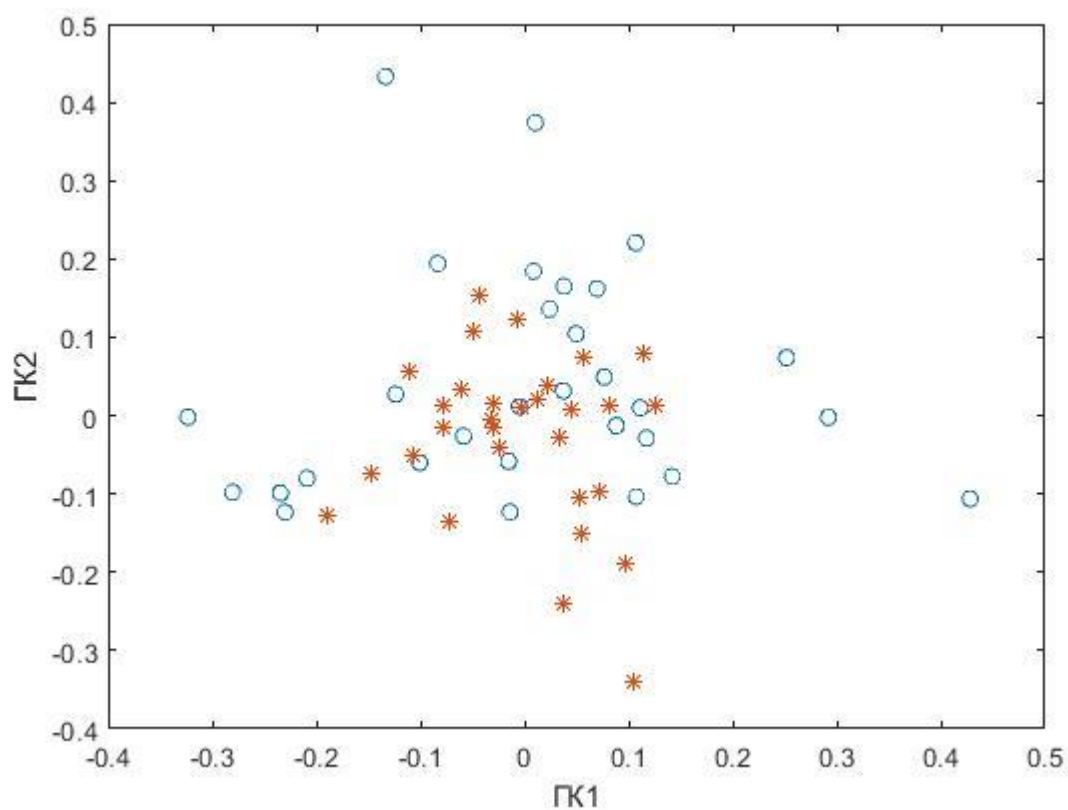


Figure 16 – PCA method with a Canny operator threshold of 0.2

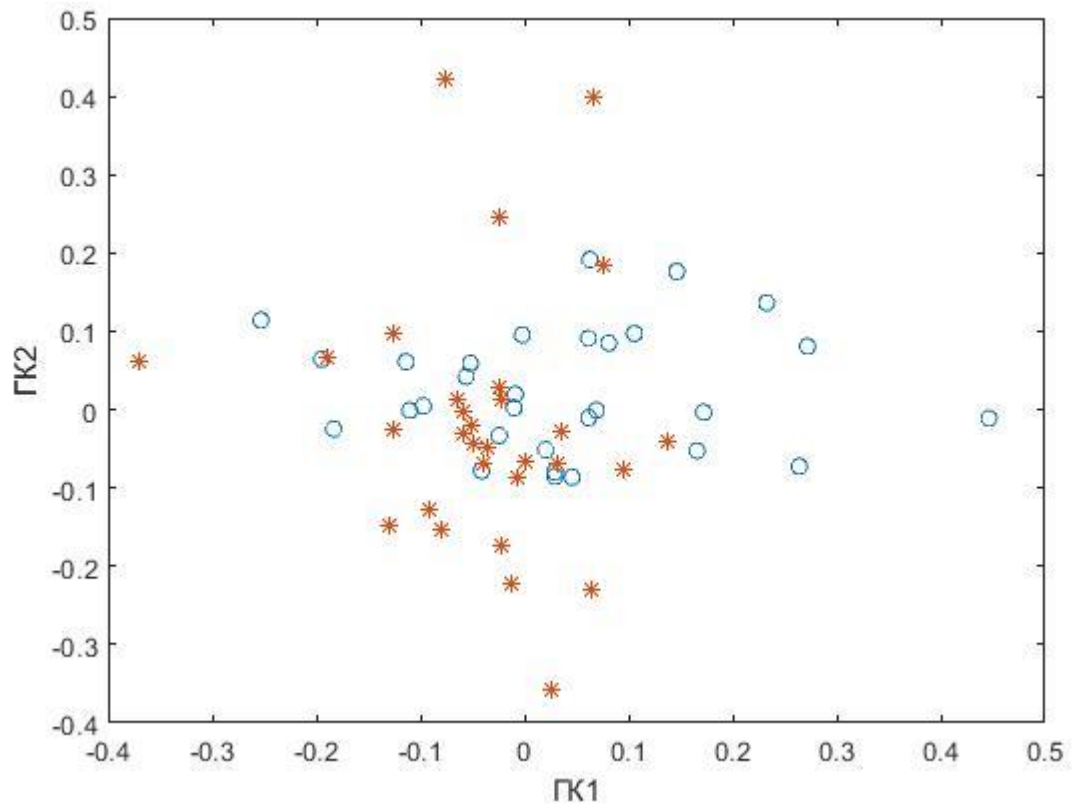


Figure 17 – PCA method with a Canny operator threshold of 0.3

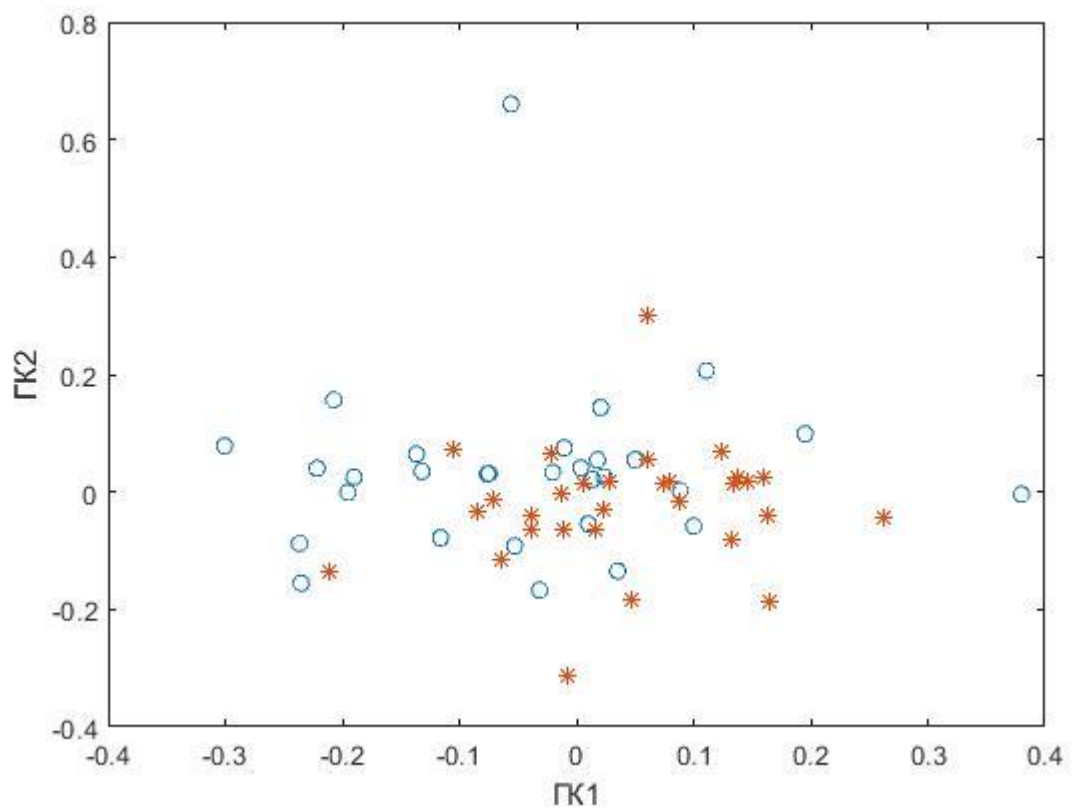


Figure 18– PCA method with a Canny operator threshold of 0.4

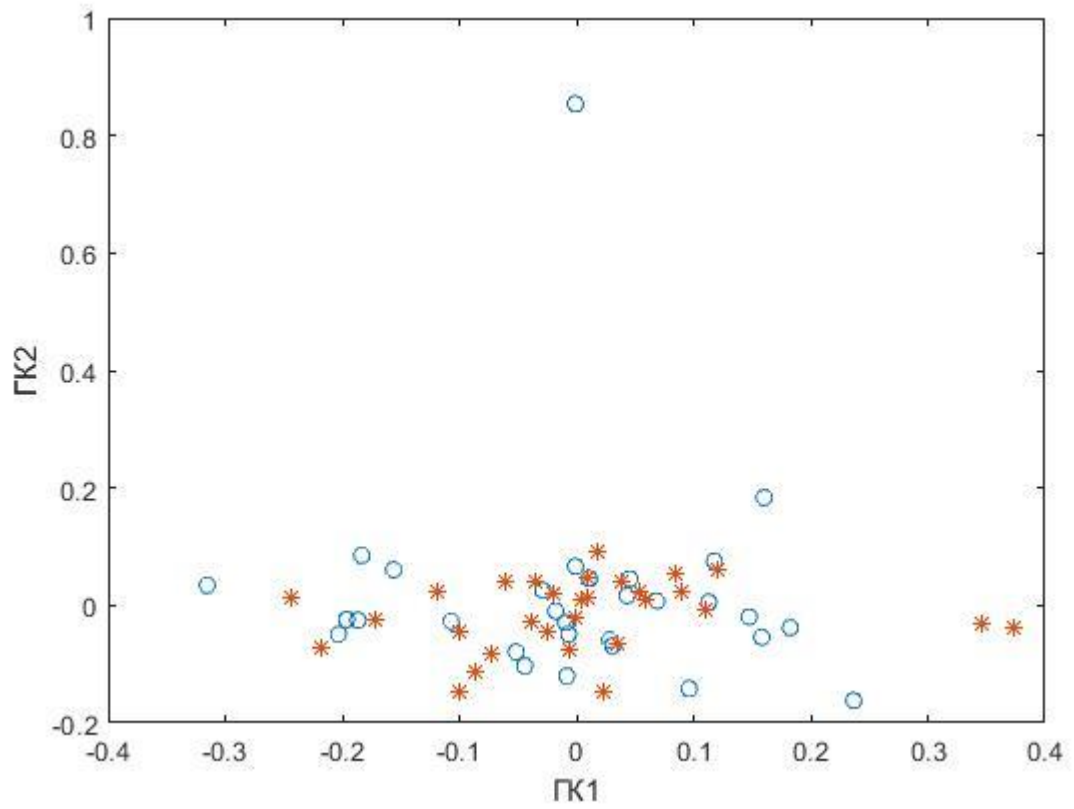


Figure 19– PCA method with a Canny operator threshold of 0.5

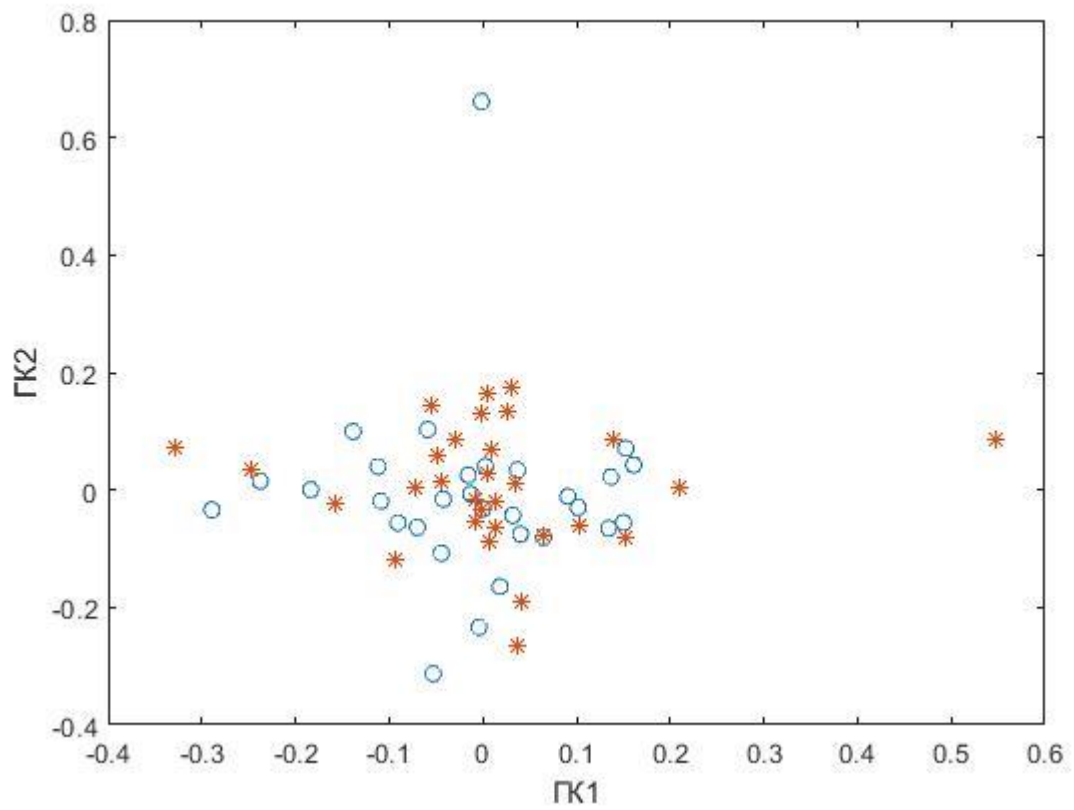


Figure 20– PCA method with a Canny operator threshold of 0.7

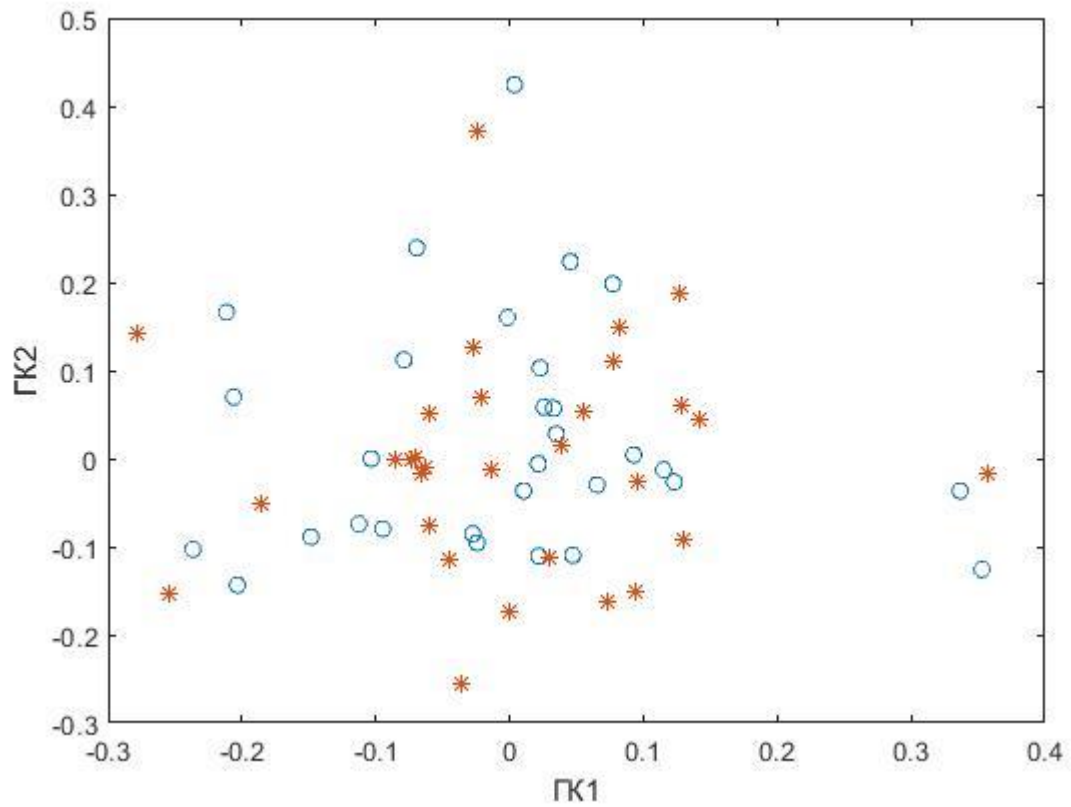


Figure 21– PCA method with a Canny operator threshold of 0.8

For comparison with the results obtained, it was decided not to use a dimensionality reduction program. As a result, the following classification of pathologies was obtained: glioblastoma – 3%, astrocytoma – 100%.

Table 2 – Result of the support vector machine using the Canny operator

Canny operator threshold value	Classified, %	
	Glioblastoma	Astrocytoma
0.1	0	93
0.2	3	100
0.3	0	93
0.4	0	93
0.5	0	93
0.6	0	93
0.7	0	96
0.8	0	96
0.9	0	96

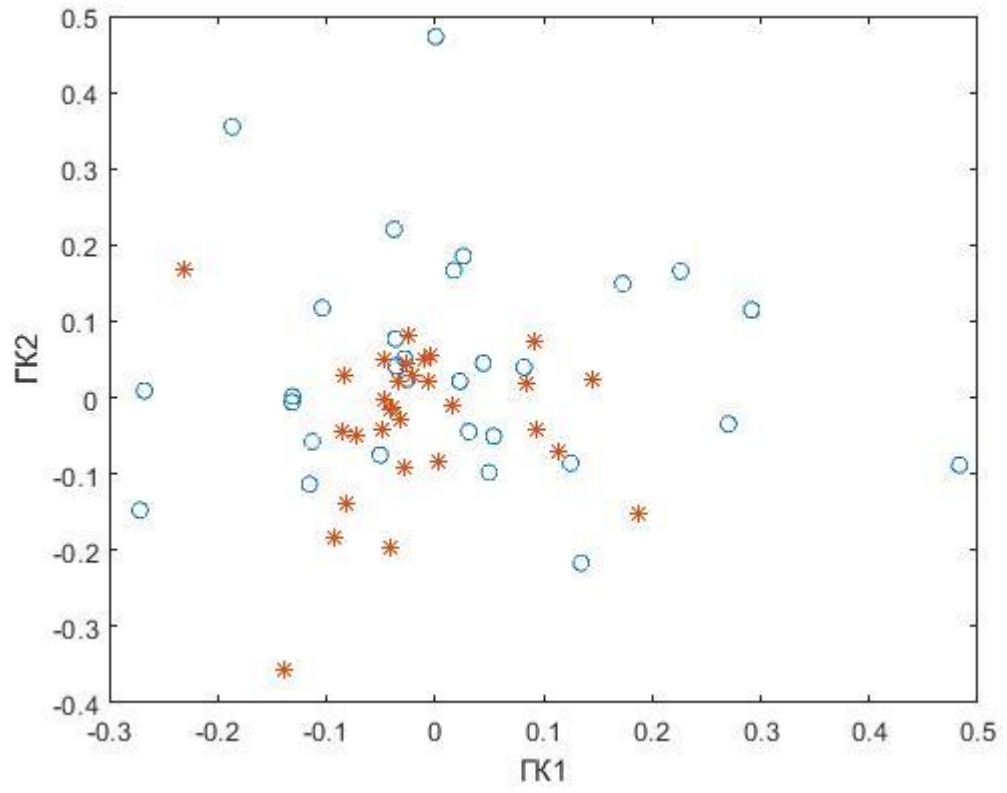


Figure 22 – The PCA method with a threshold value of the Canny operator 0.2

CONCLUSION

In the course of the work, it turned out that the best result of the classification of pathologies is: glioblastoma – 3%, astrocytoma – 100%. The best result was obtained using the Canny operator, but without the image dimension reduction program.

The reason for such results can be attributed to the criteria that were chosen for the work and the approach with reducing the dimension of images. It was found that using the program without the Canny operator gives a worse result compared to using the Canny operator. The program was also compared using the Canny, Sobel, Prewitt, Roberts operators, where the Canny operator showed the best result.

Of the two pathologies, glioblastoma is the more critical and the fact that it has been classified is an advantage of this program.

REFERENCES

1. Positron-emission tomography [Electronic resource]: Wikipedia. Free Encyclopedia. - URL: https://ru.wikipedia.org/wiki/Позитронно-эмиссионная_томография [Date of application: 12.05.2021] (in Russian)
2. Ultrasound examination [Electronic resource]: Wikipedia. Free Encyclopedia. - URL: https://ru.wikipedia.org/wiki/Ультразвуковое_исследование [Date of application: 12.05.2021] (in Russian)
3. Computed tomography [Electronic resource]: Wikipedia. Free Encyclopedia. - URL: https://ru.wikipedia.org/wiki/Компьютерная_томография [Date of application: 12.05.2021] (in Russian)
4. Magnetic resonance imaging [Electronic resource]: Wikipedia. Free Encyclopedia. - URL: https://ru.wikipedia.org/wiki/Магнитно-резонансная_томография [Date of application: 12.05.2021] (in Russian)
5. Digital Imaging and Communications in Medicine (DICOM): [Electronic resource]. URL: <http://medical.nema.org/dicom> [Date of application: 14.05.2021] (in Russian)
6. DICOM [Electronic resource]: Wikipedia. Free Encyclopedia. - URL: <https://ru.wikipedia.org/wiki/DICOM> [Date of application: 14.05.2021] (in Russian)
7. Belikova T.P. PACS: system of archiving and transmission of medical images. // Computer technology in Medicine. - 1997. - №2. - С.27-32. (in Russian)
8. Davies E.R. Machine Vision, San Diego: Academic press: 1997.
9. The Cancer Imaging Archive, TCGA-LGG. <https://wiki.cancerimagingarchive.net/display/Public/TCGA-LGG>. [Date of application: 01.04.2022]
10. Bernsen J. Dynamic thresholding of gray-level images. Proc 8th IntConf Pattern Recognition, Paris, France. 1986(October); 1251-1255.
11. Chow C.K., Kaneko T. Automatic boundary detection of the left ventricle from cineangiograms. Comput Biomed Res. 1972; 5:388 - 410.
12. Adams R., Bischof L. Seeded region growing. IEEE Trans Pattern Recogn Mach Intell. 1994; 16(6):641-647.
13. Ballard D.G., Brown C.M. Computer Vision. Englewood Cliffs: Prentice Hall; 1982.
14. Bankman I.N., Nizialek T., Simon I., Gatewood O.B., Weinberg I.N., Brody W.R. Segmentation algorithms for detecting microcalcifications in mammograms. IEEE Trans Inform Techn Biomed. 1997;1(2):141-149.

15. Singleton H.R., Pohost G.M., Automatic cardiac MR image segmentation using edge detection by tissue classification in pixel neighborhoods. *Mag Res Med*. 1997;37:418-424.
16. Hu X., Alperin N., Levin D.N., Tan K.K., Mingeot M. Visualization of MR angiography data with segmentation and volume-rendering techniques. *J Magn Res Imag*. 1001;1:539-546.
17. Lin D.T., Lei C.C., Hung S.W. Computer-aided kidney segmentation on abdominal CT images. *IEEE Trans InfTechnol Biomed*. 2006; 0(1):59-65.
18. Cline H.E., Dumoulin C.L., Hart H.R., Lorensen W.E., Ludke S. 3D reconstruction of the brain from magnetic resonance images using a connectivity algorithm. *MagnReson Imaging*. 1987;5:345-352.
19. Josofer P.H. Fundamentals of MRI: [Electronic resource]. - URL: <https://www.cis.rit.edu/htbooks/mri/inside-r.htm> [Date of application: 17.05.2021] (in Russian)
20. Pal N.R., Pal S.K. A review on image segmentation techniques. *Pattern Recognition*. 1993; 26(9):1227-1249.
21. Sonka M., Hlavac V., Boyle R. *Image Processing Analysis and Machine Vision*. Pacific Grove, CA: PWS Publishing; 1999.
22. Beucher S. Segmentation tools in mathematical morphology. *SPIE, Image Algebra and Morphological Image Processing*, 1990; 1350:70-84.
23. Roy S., Sanjay N., Maitra I. K., Bandyopadhyay S. K. A Review on Automated Brain Tumor Detection and Segmentation from MRI of Brain
24. Dogra J., Prashar N., Jain S., Sood M. Improved methods for analyzing MRI brain images//*Network Biology*, 2018, 8(1): 1-11.
25. k-means method [Electronic resource]: Wikipedia. Free Encyclopedia. - URL: https://ru.wikipedia.org/wiki/Метод_k-средних[Date of application: 20.05.2021] (in Russian)
26. Gonzales R.C., Woods R.E. *Digital Image Processing*. Reading, MA: Addison-Wesley Publishing Company; 1993.
27. GlebZakharov. What is DICOM?: [Electronic resource]. 2019. URL: <https://solutics.ru/windows/chto-takoe-fajl-dicom/> [Date of application:22.05.2021] (in Russian)
28. Read DICOM image: [Electronic resource]. URL: <https://www.mathworks.com/help/images/ref/dicomread.html>
29. Bramdt ME, Bohan TP, Kramer LA, Fletcher JM. Estimation of CSF, white and gray matter volumes in hydrocephalic children using fuzzy clustering of MR imaging. *Computerized Med Imag Graphics*. 1994; 18(1): 25-34.
30. Duda RO, Hart PE. *Pattern Recognition and Scene Analysis*, New York: Wiley; 1973.

31. Gose E, Johnsonbaugh R, Jost S. Pattern Recognition and Image Analysis. Upper Saddle River, NJ: Prentice Hall; 1996.
32. Jain AK, Flynn PJ. Image segmentation using clustering. In Bowyer K, Ahuja N, (eds.), Advances in Image Understanding. Los Alamitas, CA: IEEE Computer Society Press; 1996.
33. Mitiche A, Aggarwal JK. Image segmentation by conventional and information-integrating techniques: A synopsis. Image and Vision Computing. 1985; 3(2):50-62.
34. Pratt WK. Digital Image Processing. New York: John Wiley & Sons; 1991.
35. Marr D, Hildreth E. Theory of edge detection. Proc Roy Soc London. 1980; 187-217.
36. Brenner JF, Jester JM, Selles WD. Scene segmentation in automated histopathology: Techniques evolved from cytology automation. Pattern Recognition. 1981; 13:65-77.
37. Gonzalez RC, Woods RE. Digital Image Processing. Reading, MA: Addison-Wesley Publishing Company; 1993.
38. Sonka M., Reddy GK, Winniford MD., Collins SM. Adaptive approach to accurate analysis of small-diameter vessels in cineangiograms. IEEE Trans Med Imag. 1997; 16(1):87-95.
39. Rogowska J, Bryant CM, Brezinski ME. Cartilage Thickness measurements from optical coherence tomography. J Opt Soc Am A Opt Image Sci Vis. 2003; 20(2):357-367.
40. Castleman KR. Digital Image Processing. Upper Saddle River: Prentice Hall; 1996.
41. Ballard DG, Brown CM. Computer Vision. Englewood Cliffs: Prentice Hall; 1982.
42. Gerig G, Kubler O, Kikinis R, Jolesz FA. Nonlinear anisotropic filtering of MRI data. IEEE Trans Med Imag. 1992;11(2):221-232.
43. Haralick RM, Shapiro LG. Survey: Image segmentation techniques. Comp Vision Graph Image Proc. 1985;29:100-32.
44. Rosenfeld A, Kak AC. Digital Image Processing. New York: Academic Press; 1982.
45. Principal component analysis [Electronic resource]: Wikipedia. Free Encyclopedia. - URL: https://ru.wikipedia.org/wiki/Метод_главных_компонент [Date of application: 19.02.2022]. (in Russian)

46. Johnson LA, Pearlman JD, Miller CA, Young TI, Thulborn KR. MR quantification of cerebral ventricular volume using a semiautomated algorithm. *AJNR*. 1993;14:1313-1378.
47. Preston K, Duff MJ. *Modern Cellular Automata*. New York: Plenum Press; 1984.
48. Chow CK, Kaneko T. Automatic Boundary detection of the left ventricle from cineangiograms. *Comput Biomed Res*. 1972;5:388-410.
49. Davies ER. *Machine Vision*, San Diego: Academic Press; 1997.
50. Bomans M, Hohne KH, Tiede U, Riemer M. 3-D segmentation of MRI images of the head for 3-D display. *IEEE Trans Medical Imaging*. 1990;9(2):177-183.
51. Higgins WE, Ojard EJ. Interactive morphological watershed analysis for 3D medical images. *Proceedings of the Symposium on 3D Advanced Image Processing in Medicine*. Rennes, France. 1992(Nov. 2-4):117-121.
52. Hall LO, Bensaid AM, Clarke LP, Velthuizen RP, Silbiger MS, Bezdek JC. A comparison of neural network and fuzzy clustering techniques in segmenting magnetic resonance images of the brain. *IEEE Trans Neural Networks*. 1992;3(5):672-682.
53. Rogowska J, Brezinski ME. Image processing techniques for noise removal, enhancement and segmentation of cartilage OCT images. *Phys Med Biol*. 2002;47(4):641-655.
54. Yan J, Zhao B, Curran S, Zelenetz A, Schwartz LH. Automated matching and segmentation of lymphoma on serial CT examinations. *Med Phys*. 2007;34(1):55-62.
55. Grau V, Mewes AU, Alcaniz M, Kikinis R, Warfield SK. Improved watershed transform for medical image segmentation using prior information. *IEEE Trans Med Imaging*. 2004;23(4):447-458.
56. Wang JZ, Turner DA, Chutuape MD. Fast, interactive algorithm for segmentation of series of related images: Application to volumetric analysis of MR images of the heart. *JMRI*. 1992;2(5):575-582.
57. Marr D, Hildreth E. Theory of edge detection. *Proc Roy Soc London*. 1980;27:187-217.
58. Cline HE, Lorensen WE, Kikinis R, Jolesz R. Three-dimensional segmentation of MR images of the head using probability and connectivity. *J Comp Assisted Tomography*. 1990;14(6):1037-1045.
59. Reddick WE, Glass JO, Cook EN, Elkin TD, Deaton RJ. Automated segmentation and classification of multispectral magnetic resonance images of brain using artificial neural networks. *IEEE Trans Med Imag*. 1997; 16(6):911-918.
60. Held K, Rota Kopps E, Krause B, Wells W, Kikinis R, Muller-Gartner H. Markov random field segmentation of brain MR images. *IEEE Trans Med Imag*. 1998;16:878-887.

61. Gerig G, Martin J, Kikinis R, Kuebler O, Shenton M, Jolesz FA. Automating segmentation of dual-echo MR head data. In Colchester AC, Hawkes DJ (eds.), *Information Pricessing in Medical Imaging*. Berlin: Springer-Verlag; 1991:175-185.
62. Warfield SK, Kaus M, Jolesz FA, Kikinis R. Adaptive template moderated spatially varying statistical classification. In Wells WM, Colchester A, Delp S, (eds.), *Proc of First IntConf on Medical Image Computing and Computer-Assisted Intervention (MICCAI)*. Lecture Notes in Computer Science. Springer-Verlag, 1998:431-438.
63. Gerig G, Kubler O, Kikinis R, Jolesz FA. Nonlinear anisotropic filtering of MRI data. *IEEE Trans Med Imag*. 1992;11(2):221-232.
64. Guillemaud R, Brady M. Estimating the bias field of MR images. *IEEE Trans Med Imag*. 1997;16(3):238-251.
65. Kapur T, Grimson WEL, Kikinis R, Wells WM. Enhanced spatial priors for segmentation of magnetic resonance imagery. In Wells WM, Colchester A, Delp S, (eds.), *Proc. of First Int. Conf. on Medical Image Computing and Computer-Assisted Intervention (MICCAI)*. Lecture Notes in Computer Science. Springer-Verlag, 1998:457-468.
66. Nagata K, Asano T. Functional image of dynamic computed tomography for the evaluation of cerebral hemodynamics. *Stroke*. 1990;21:882-889.
67. Gerig G, Welte D, Guttman C, Colchester A, Szekely G. Exploring the discrimination power of the time domain for segmentation and characterization of lesions in serial MR data. In Wells WM, Colchester A, Delp S, (eds.), *Proc of First Intern Conf on Medical Image Computing and Computer-Assisted Intervention (MICCAI)*. Lecture Notes in Computer Science. Springer-Verlag, 1998:469-479.
68. Rogowska J. Similarity methods for dynamic image analysis. *Proceedings of International Conf of AMSE*. 1991;2:113-124.
69. Bandettini PA, Jesmanowicz A, Wong EC, Hyde JS. Processing strategies for functional MRI of the human brain. *Magn Res Med*. 1993;30:161-173.
70. Zucker SW. Region growing: Childhood and adolescence. *Comp Graphics Image Proc*. 1976;5:382-399.
71. Fu KS, Mui JK. A survey on image segmentation. *Pattern Recognition*. 1981;13(1):3-16.
72. Taxt T, Lundervold A, Fuglaas B, Lien H, Abeler V. Multispectral analysis of uterine corpus tumors in magnetic resonance imaging. *Magn Res Med*. 1992;23:55-76.
73. Clinical recommendations: Primary tumors of the central nervous system/composition for the development and revision of clinical recommendations: T. R.

Izmailov [et al.].-All - Russian National Union "Association of Oncologists of Russia ", 2019. (in Russian)

74. Rogowska J, Batchelder K, Gazelle GS, Halpern EF, Connor W, Wolf GL. Quantitative CT lymphography: Evaluation of selected two-dimensional techniques for computed tomography quantitation of lymph nodes. *Investigative Radiology*. 1996;31(3):138-145.

75. Vincen L, Soille P. Watersheds in digital spaces: An efficient algorithm based on immersion simulations. *IEEE Trans PAMI*. 1991;13(6):583-598.

76. Rogowska J. Digital image processing techniques for speckle reduction, enhancement and segmentation of optical coherence tomography (OCT) images. In Brezinski M, (ed.), *Optical Coherence Tomography*. Elsevier; 2006.

77. Support vectors machine [Electronic resource]: Wikipedia. Free Encyclopedia. - URL: https://ru.wikipedia.org/wiki/Метод_опорных_векторов [Date of application: 04.05.2022] (in Russian)

78. The Cancer Imaging Archive, Brain-Tumor-Progression. <https://wiki.cancerimagingarchive.net/display/Public/Brain-Tumor-Progression>. [Date of application: 14.05.2021]

79. Alexey Pomerantsev. Principal component analysis // Russian Chemometric Community. [Electronic resource], 2008. URL: <https://www.chemometrics.ru/old/Tutorials/pca.htm>

Отчет о проверке на заимствования №1



Автор: Altynbekov Almat Altynbekovich
Проверяющий: Касаткина Анна Наильевна (ane4ka.com.ru@sibmail.com / ID: 644)
Организация: Томский Государственный Университет

Отчет предоставлен сервисом «Антиплагиат» - <http://tsu.antiplagiat.ru>

ИНФОРМАЦИЯ О ДОКУМЕНТЕ

№ документа: 80
 Начало загрузки: 09.06.2022 11:05:21
 Длительность загрузки: 00:00:09
 Корректировка от 09.06.2022 11:10:07
 Имя исходного файла:
 Master_s_Thesis_Altynbekov_final.pdf
 Название документа:
 Master_s_Thesis_Altynbekov_final
 Размер текста: 1 кБ
 Символов в тексте: 82826
 Слов в тексте: 12350
 Число предложений: 684

ИНФОРМАЦИЯ ОБ ОТЧЕТЕ

Последний готовый отчет (ред.)
 Начало проверки: 09.06.2022 11:05:30
 Длительность проверки: 00:03:33
 Комментарии: [Автосохраненная версия]
 Поиск с учетом редактирования: да
 Модули поиска: ИПС Адилет, Библиография, Сводная коллекция ЭБС, Интернет Плюс, Сводная коллекция РГБ, Цитирование, Переводные заимствования (RuEn), Переводные заимствования по eLIBRARY.RU (EnRu), Переводные заимствования по Интернету (EnRu), Переводные заимствования издательства Wiley (RuEn), eLIBRARY.RU, СПС ГАРАНТ, Медицина, Диссертации НББ, Перефразирование по eLIBRARY.RU, Перефразирование по Интернету, Патенты СССР, РФ, СНГ, СМИ России и СНГ, Шаблонные фразы, Модуль поиска "ТГУ", Кольцо вузов, Издательство Wiley, Переводные заимствования



ЗАИМСТВОВАНИЯ

28,63%

САМОЦИТИРОВАНИЯ

0%

ЦИТИРОВАНИЯ

0%

ОРИГИНАЛЬНОСТЬ

71,37%

Заимствования — доля всех найденных текстовых пересечений, за исключением тех, которые система отнесла к цитированиям, по отношению к общему объему документа.
 Самоцитирование — доля фрагментов текста проверяемого документа, совпадающий или почти совпадающий с фрагментом текста источника, автором или соавтором которого является автор проверяемого документа, по отношению к общему объему документа.
 Цитирования — доля текстовых пересечений, которые не являются авторскими, но система посчитала их использование корректным, по отношению к общему объему документа. Сюда относятся оформленные по ГОСТу цитаты; общепотребительные выражения; фрагменты текста, найденные в источниках из коллекций нормативно-правовой документации.
 Текстовое пересечение — фрагмент текста проверяемого документа, совпадающий или почти совпадающий с фрагментом текста источника.
 Источник — документ, проиндексированный в системе и содержащийся в модуле поиска, по которому проводится проверка.
 Оригинальность — доля фрагментов текста проверяемого документа, не обнаруженных ни в одном источнике, по которым шла проверка, по отношению к общему объему документа.
 Заимствования, самоцитирование, цитирования и оригинальность являются отдельными показателями и в сумме дают 100%, что соответствует всему тексту проверяемого документа.
 Обращаем Ваше внимание, что система находит текстовые пересечения проверяемого документа с проиндексированными в системе текстовыми источниками. При этом система является вспомогательным инструментом, определение корректности и правомерности заимствований или цитирований, а также авторства текстовых фрагментов проверяемого документа остается в компетенции проверяющего.